Summer 7-2014

Aerosol Association with Severe Weather in the Great Plains

Gabriel A. Lojero
University of Nebraska-Lincoln, galojero@gmail.com

AEROSOL ASSOCIATION WITH SEVERE WEATHER IN THE GREAT PLAINS

by

Gabriel A. Lojero

A THESIS

Presented to the Faculty of

The Graduate College at the University of Nebraska

In Partial Fulfillment of Requirements

For the Degree of Master of Science

Major: Earth and Atmospheric Sciences

Under the Supervision of Professor Matthew S. Van Den Broeke

Lincoln, Nebraska

July, 2014

AEROSOL ASSOCIATION WITH

SEVERE WEATHER IN THE GREAT PLAINS

Gabriel Alberto Lojero, M.S.

University of Nebraska, 2014

Adviser: Matthew S. Van Den Broeke

Aerosols particles may serve as cloud condensation nuclei (CCN) and therefore play an important role in modulating cloud microphysics, to the point where convective storm intensity may be altered. The purpose of this study is to determine the impacts of biomass burning aerosols on convective storms over the Great Plains, especially the southern Great Plains, and to show synoptic regimes characterizing differing aerosol concentrations. A new technique to identify days with a high concentration of biomass burning aerosols was developed by using organic carbon, potassium, zinc, and bromine as the predominant tracers. An eleven-year climatology (2002-2012) for the biomass burning tracers was produced to identify days on which biomass burning particles were present, and an average concentration of these tracers was obtained from two different sensors in western Oklahoma: Ellis and Wichita Mountains. Once prevalence of biomass burning particles was identified for each day, days were classified into high (upper 30%), medium (middle 40%), and low (lowest 30%) biomass burning particle concentration. Only March through June was considered since this is climatologically the convective season in the Southern Great Plains. Days with severe thunderstorms and with similar

thermodynamic (CAPE) and kinematic (shear) environments were chosen as case study days, from which storm report data were obtained and compared. Additionally, composite synoptic regime and a set of trajectories were obtained for each aerosol concentration category. Lastly, differential reflectivity and correlation coefficient values were examined to compare the microphysics of thunderstorms occurring on days of different aerosol concentration. Case studies of High Plains and Oklahoma storms were examined. This study is one of the first observational studies to examine aerosol effects on convective storms in the Great Plains region.

Acknowledgements

The work presented would have not been possible without the suggestions, guidance, and encouragement of many. I would first like to thank my advisor, Dr. Matthew Van Den Broeke, who frequently provided the knowledge that greatly increased my understanding of the polarimetric radar variables and who guided me through the research process. I would also like to thank my committee members, Dr. Adam Houston and Dr. Jun Wang, for their superb insight and knowledge as I went through the research process. I would also like to express thanks to the Department of Earth and Atmospheric Sciences at the University of Nebraska-Lincoln for providing me with a teaching assistantship that helped cover the costs to attend graduate school and complete this project.

Many people have supported and encouraged me along the way through graduate school, especially my graduate school colleagues. I would like to give a special thanks to my parents, who have always provided encouragement and reassurance in my academic pursuits. Without their guidance and support, I would not be in this position.

Table of Contents

List of Figures

1. Introduction

Depending on supersaturation and particle size, aerosol particles can act as cloud condensation nuclei (CCN) and may therefore alter cloud microphysics (e.g., Rose et al. 2010). Clouds forming in regions of high CCN concentration have been observed to contain higher concentration of small cloud droplets (Twomey 1974), suppressing precipitation and delaying the warm-rain process. This increases cloud water content, leading to higher liquid droplet and ice crystal number concentration, which enhances latent heat release and helps invigorate convection (Rosenfeld 1999; Andreae et al. 2004; Lin et al. 2006; Yuan et al. 2011; Rosenfeld and Bell 2011).

Even though many studies have examined the effects of aerosols on convective invigoration, there have been few detailed observational studies performed over the Great Plains of the United States, one of the most active convective regions in the world. Therefore, we seek to provide a preliminary observational study of aerosol effects on convection over the Great Plains, using storm reports and radar data.

A major source of aerosols reaching the Southern Great Plains is from the emission of biomass burning particles from wildfires in Central America, especially southern Mexico and the Yucatan Peninsula. These wildfires are common during the northern tropical dry season which runs from March to early June (Reid et al. 2004; Wang et al. 2006). Wang et al. (2009) reported that the ideal synoptic conditions needed to transport smoke particles into the Southern Great Plains from this source region include strong southerly airflow from the Gulf of Mexico at low-levels, produced in the presence of an

approaching mid-latitude trough carrying a southward-moving cold front along with a Bermuda high to the east. In this study, we seek to provide a detailed analysis of the synoptic patterns and parcel path trajectories most common during days characterized by different aerosol concentrations.

As many have hypothesized, aerosols play an important role in modulating the cloud microphysics. No previous studies have looked at microphysical differences in thunderstorms between days of significantly different aerosol concentration for mid-latitude locations. Therefore, we seek to describe the differences in the microphysics of storms using polarimetric radar data by examining both High Plains and Southern Plains cases.

Chapter 2 provides relevant background information applicable for this study. In chapter 3, the data and methodology used to obtain the results are discussed. Chapter 4 examines how the distribution of storm reports changes as a function of aerosol concentration. Chapter 5 provides a presentation of the overall synoptic regimes and parcel path trajectories leading up to days of different aerosol concentration. Chapter 6 provides an overview of microphysical differences in thunderstorms from days of different aerosol concentration, while chapter 7 provides an overview of the most important conclusions of this study.

1. Background

I. Source Region of Biomass Burning Particles in the Southern Great Plains

A major source of aerosols reaching the Southern Great Plains is from the emission of biomass burning particles from the wildfires of Central America, especially the Yucatan Peninsula. Wang et al. (2006) found that smoke particles from wildfires in Mexico produced a 40-60% increase in the monthly average of particulate matter with diameter 2.5 micrometers or less (PM2.5) concentration over east and south Texas during April and May of 2003. Wang et al. (2009) reported that smoke particle transport from the Yucatan Peninsula into the Southern Great Plains is facilitated by having strong southerly airflow from the Gulf of Mexico at low levels, which is produced in the presence of an approaching mid-latitude trough along with a Bermuda high to the east. This combination of the approaching mid-latitude trough with Bermuda high helps to intensify the warm conveyor belt, which acts as a forcing mechanism for convection initiation (Wang et al. 2009). The warm conveyor belt can also act as lifting mechanism for smoke particles to be transported from the boundary layer to the free troposphere (Fig. 2.1). Even in the absence of long-range transport, aerosol concentration in the Southern Great Plains could also be high due to local wildfires and duststorms occurring during dry years.

II. Aerosol Effects on Storm Invigoration

Not all aerosol particles can effectively serve as CCN. Rose et al. (2010) measured CCN particles in polluted air and biomass burning smoke for a one-month period at a rural site in southeastern China. They found that particles in polluted air and biomass burning smoke being effective CCN depended on the water vapor supersaturation *(S)* and aerosol particle size. The higher *S* was, the higher the CCN number concentration (from 1000 cm^{-3} at $S = 0.068\%$ to 16000 cm^{-3} at $S = 1.27\%$). A lower *S* required larger particle sizes for activation.

Aerosols have been hypothesized to have significant effects on clouds, including invigoration. Bell et al. (2008) examined this effect by providing evidence that a midweek increase in rainfall during the summer months resulted from a midweek maximum in aerosol concentration. By examining EPA measurements of PM2.5 or 10 micrometers or less (PM10), they found a midweek peak of these particulates over the southeastern U.S. By using the Tropical Rainfall Measuring Mission (TRMM) satellite estimates of rainfall, a midweek peak in rainfall and cloud top height in thunderstorms was found, mainly over the southeastern U.S., which was statistically significant relative to weekends. Bell et al. (2008) define storm height as the height of the highest point of the radar beam with a detectable return (~17-18 dBZ) measured relative to sea-level. Using the NCEP reanalysis data, a weekly cycle of convergence at 1000 hPa, upward vertical motion, and divergence at 300 hPa was noted. As a follow-up to this study, Bell et al. (2009) looked into the weekly cycle of lightning during the summer months (June to

August) from 1998-2006 to examine if the same pattern were noted. A weekly cycle of lightning activity was noted over the southeastern U.S., and this cycle was more notable during the afternoon when convective potential is highest. In addition, Bell et al. (2009) examined whether this weekly cycle of lightning activity was due to a weekly modulation of the synoptic pattern, and no strong evidence was found. Rosenfeld and Bell (2011) examined whether the same pattern noted with rain and storm heights (Bell et al. 2008) and lightning (Bell et al. 2009) was evident with tornadoes and hailstorms. Using tornado and hail reports from 1995-2009 during the months of June through August east of 100°W, they found a weekly cycle of tornadoes and hailstorms, which coincided with the weekly aerosol cycle. Lerach et al. (2008) performed numerical simulations of an idealized supercell thunderstorm to study the effects of increased aerosol concentration on tornadogenesis using a two-moment bulk microphysics scheme. It was found that the polluted environment produced a longer-lived supercell with a well-defined rear flank downdraft and a tornado-like vortex of EF-1 intensity. Lerach et al. (2008) argued that higher aerosol concentration reduced the warm and cold rain process within the rear-flank and forward-flank downdraft, reducing precipitation rates. A low evaporative cooling rate produced a weaker cool pool that did not surge outward, allowing for the low-level mesocyclone and the near-surface vorticity produced by the rear flank downdraft gust front to remain vertically-stacked. Along the same lines, Learch and Cotton (2012) compared aerosol and low-level moisture influences on supercell tornadogenesis using three-dimensional idealized simulations. It was found that the polluted scenario was associated with weaker cold pools and less negative buoyant air within the rear-flank

downdraft as the raindrop and hail concentrations were reduced, which would prove to more favorable for tornadogenesis. Learch and Cotton (2012) argued, however, that even though an aerosol effect was evident that low-level moisture quantity and instability had far greater effects on tornadogenesis. Khain et al. (2010) performed a study, using a bin microphysical modeling scheme, of the impacts of CCN concentration on hail size. An increase in hail mass and size was noted as CCN concentration increased. Khain et al. (2010) proposed that the mechanism favoring this result was an increase in CCN concentration leading to an increase in supercooled water aloft, increasing riming efficiency. This leads to the formation of larger graupel and hail particles.

A major fire episode occurred over Mexico during the spring of 1998 and smoke was transported northward into the U.S. Great Plains and southern Canada. Lyons et al. (1998) found that smoke from these fires appeared to have a substantial effect on the electrical characteristics of thunderstorms occurring over the Great Plains. It was found that the percentage of positive cloud-to-ground lightning within thunderstorms increased substantially during the spring of 1998, with the greatest increase noted during mid-May when the smoke concentration was at its greatest (Fig. 2.2). The large increase in positive cloud-to-ground lightning is most likely due to greater number concentration of ice crystals aloft. It has been hypothesized that greater aerosol concentration leads to small cloud droplets, delaying the warm rain process and allowing more cloud water to be transported vertically to form a higher number concentration of liquid droplets and ice crystals aloft (Rosenfeld 1999; Andreae et al. 2004; Lin et al. 2006; Wang et al. 2009;

Rosenfeld and Bell 2011). Yuan et al. (2011) found an increase in lightning activity during 2005 in the West Pacific east of the Philippines. This was the same year that volcanic activity was noted in the region, causing increased aerosol loading. Using the Moderate Resolution Imaging Spectroradiometer (MODIS), it was concluded that a 60% increase in aerosol loading due to volcanic activity led to a 150% increase in lightning activity as noted by the Lightning Imaging Sensor aboard the TRMM. It was noted that this dramatic increase in lightning activity in 2005 was neither a result of an interannual variability of large-scale synoptic conditions or a result of a few extreme active periods during the year. Yuan et al. (2011) also found that the glaciation temperature in 2005 was the coldest of all the years and 8°C colder than the warmest year, translating to a 1-2 km height increase in the glaciation level.

III. Aerosol Loading Effects on Cloud Microphysics

In recent decades, several studies have looked at the effects of aerosol loading on cloud microphysics. Twomey (1974) argued that an increase in air pollution caused a significant increase in cloud condensation nuclei (CCN) and cloud albedo. It was also noted that CCN concentration was noticeably lower over the ocean where air pollution concentration was lower. Albrecht (1989) reported from measurements obtained from aircraft flying through horizontal homogeneous oceanic clouds that an inverse relationship existed between droplet concentration and mean volume radius (Fig. 2.3). Kauffman et al. (2005) examined four different regions of the Atlantic Ocean to

investigate the effects of air pollution on shallow cloud development. Using MODIS to track aerosol concentration, it was found that as the aerosol optical thickness increased, the stratiform cloud coverage increased and the cloud droplet radius decreased. Furthermore, Yuan et al. (2011) found that in 2005, during volcanic activity in the West Pacific east of the Philippines when aerosol thickness increased by 60%, droplet radius inside deep convective storm clouds was about 2 micrometers lower compared to other years.

Several studies have examined the effects of aerosol loading on suppressing precipitation until cloud tops reach significantly higher altitudes. Rosenfeld (1999) used TRMM satellite observations and noted that smoke from forest fires in Indonesia may inhibit rainfall. Observations were compared between clouds in a smoky environment and clouds in a clean environment. Using the droplet radius threshold for precipitation formation as 14 micrometers, Rosenfeld (1999) observed that the threshold for the clouds in the clean environment was achieved at -8°C while with clouds in the smoky environment the threshold was achieved at -12°C. This was an indication that precipitation in the smoky environment was suppressed until the cloud tops reached a higher altitude. Rosenfeld (1999) argued that the reason for this difference was that smoke-filled clouds have droplets small enough to not coalesce into precipitation until reaching higher altitudes. Battan and Braham (1956) compared radar echoes of oceanic vs. continental clouds by examining oceanic clouds off the coast of Puerto Rico and continental clouds in the central U.S. They noted that radar echoes first appeared from

oceanic clouds with tops as low of 2000 m, whereas radar echoes first appeared from the continental clouds with substantially higher cloud tops, 4000 m.

Li et al. (2011) examined the impacts of aerosols on the vertical development of clouds and precipitation using a 10-year dataset of cloud, aerosol, and meteorological variables collected in the Southern Great Plains region. All of these observations were ingested into the Weather Research and Forecasting Model (WRF) that was coupled with a spectral-bin microphysics scheme (see Li et al. 2011) and simulations were performed. Mixed-phase clouds (containing both liquid water and ice) with a warm base (cloud base temperature greater than 15°C) had a lower cloud top temperature as CCN concentration increased. This trend was more noticeable during the summer, when cloud bases tend to be warm. Cloud thickness during the summer also increased as CCN concentration increased. Rainfall frequency and amount were also higher with higher CCN concentration.

Khain et al. (2005) examined the aerosol effects on the dynamics and microphysics of deep convection by comparing a maritime and a continental environment with the assumption that a continental environment contains a higher aerosol concentration due to a higher CCN concentration. They found that since droplet size is smaller in continental clouds, the collision efficiency is not as great so droplets ascend to higher levels within the cloud. Therefore, more droplets are able to freeze, increasing the latent heat release aloft, which increases the updraft strength. In this experiment, Khain et al. (2005) also

found an increase in downdraft strength in continental clouds due to greater sublimation of ice and evaporation of droplets.

More recent modeling results have been obtained on the effect of aerosol variability on convective microphysics. Mansell and Ziegler (2013) examined the effects of aerosols on simulated storm electrification using a two-moment bulk microphysics model. It was found that as CCN concentration increased from 50 to about 2000 cm^{-3}, graupel production and lightning activity increased. Storer and Van den Heever (2013) examined the effects of aerosol on the microphysics of tropical deep convective clouds. It was found that in the polluted simulations, more deep convective clouds, wider storms, higher cloud tops, and more convective precipitation was common. It was also found that in the polluted simulations more extreme values of vertical velocity were observed, however, a decrease in updraft strength was also observed in cloud tops greater than 6 km. Storer and Van den Heever (2013) argued that the reason that updraft strength may have decreased in cloud with tops greater than 6 km is that at this point condensate loading becomes a factor to the point of reducing the updraft strength. May et al. (2011) examined the impacts of aerosols on drop size distributions in tropical thunderstorms occurring in the islands north of Darwin, Australia using polarimetric radar observations. It was found that in high aerosol concentration regimes, there was a smaller number concentration of larger drops.

Many studies have shown that the effects of aerosols on precipitation depend on the relative humidity within the cloud environment. An increase in aerosol concentration

increases both the generation and loss of condensate mass (Khain et al. 2008). In a cloud environment with high relative humidity, aerosols tend to produce an increase in precipitation (Khain et al. 2005, 2008; Lynn et al. 2005, 2007; Tao et al. 2007), while in a cloud environment with a lower relative humidity, increasing aerosol concentration tends to produce a decrease in precipitation (Givati and Rosenfeld 2004; Jirak and Cotton 2006; Lynn et al. 2007). In an environment with high relative humidity, condensate production is increased, leading to increased precipitation. In an environment with lower relative humidity, condensate production is reduced, leading to decreased precipitation.

IV. Recent Controversy Surrounding Aerosol Effects on Cloud Microphysics

The Rosenfeld and Bell (2011) paper on the weekly cycle of tornadoes and hailstorms initiated a lively debate in the severe storms community. Yuter et al. (2013) argued that the conclusion of Rosenfeld and Bell (2011) that aerosols can influence tornadoes and hailstorms is not applicable for supercell thunderstorms. It was argued that due to the complexity of supercell thunderstorms, it was inconclusive to link aerosols to the outflow temperature near a tornado. Since the bounded weak echo region (BWER) of a supercell is usually a region where the strongest updrafts tend to reside and where the radar reflectivity is a minimum, Yuter et al. (2013) argued that supercell updrafts have little time for droplet growth and that the conditions needed to obtain large supercooled liquid water content for hail growth is present even without the need to invoke any aerosol influences. In a response, Rosenfeld and Bell (2013) argued that the arguments of Yuter

et al. (2013) on the lack of precipitation in the BWER are irrelevant as aerosols control the formation of most of the precipitation embryos and therefore their accretion efficiency with cloud drops as cloud drop sizes are being modulated by aerosols. Yuter et al. (2013) argued that the conclusion of Rosenfeld and Bell (2011) on hail size is an over-simplification of the understanding of the bulk hail population as hailstones take on several trajectories within supercells. Even though model simulations have found that hail mass and hail diameter increases as CCN concentration increases using bin microphysics and the opposite situation occurs using bulk microphysics, Yuter et al. (2013) argued that the effects of aerosol on hail size is unpredictable due to the complexity of hailstone growth. Rosenfeld and Bell (2013) argued, however, that if a model is run using bulk microphysics that it would not be able to fully capture the size distributions of the various cloud and hydrometer species as argued by Khain et al. (2010). Yuter et al. (2013) also argued based on theory and experimental data for hailstone embryo growth performed by Cober and List (1993) that smaller cloud droplets have significantly smaller collection efficiencies, making it more difficult for hailstones to grow in diameter, which Rosenfeld and Bell (2013) argued was due to less physically-based numerical calculations. This research will seek to present additional evidence for or against aerosol invigoration of deep convection by showing additional observational data from which the presence or absence of an aerosol effect may be assessed.

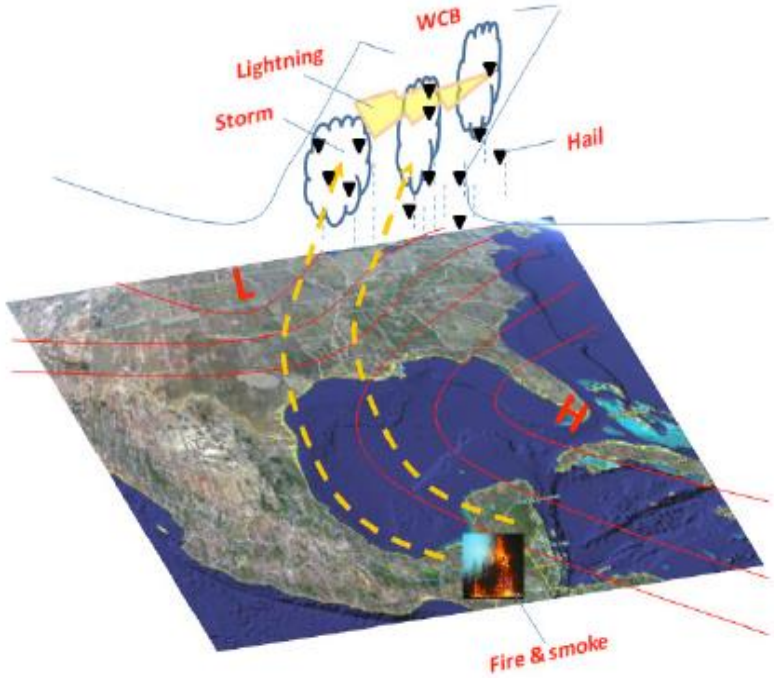

Figure 2.1: Wang et al. (2009) conceptual model of the synoptic regime most favorable for the transport of smoke particles from the Yucatan Peninsula and interact with storm clouds over the south-central U.S.

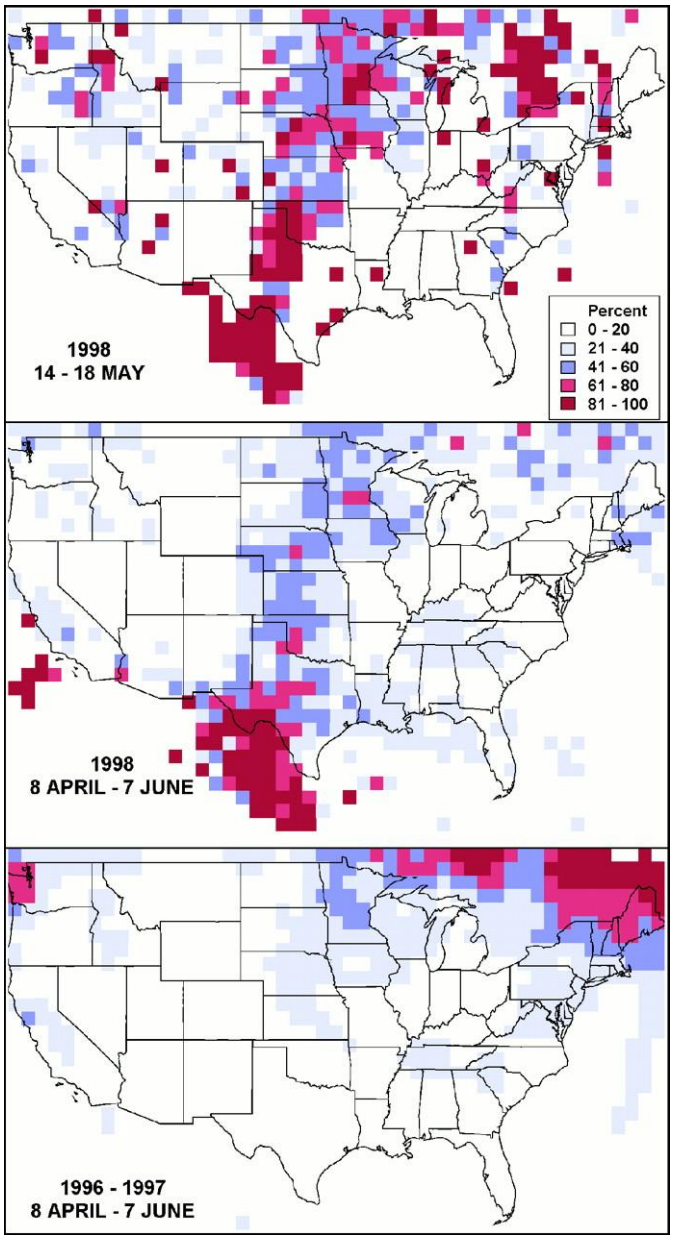

Figure 2.2: Lyons et al. (1998) map showing the percentage of positive cloud to ground lightning strikes within thunderstorms.

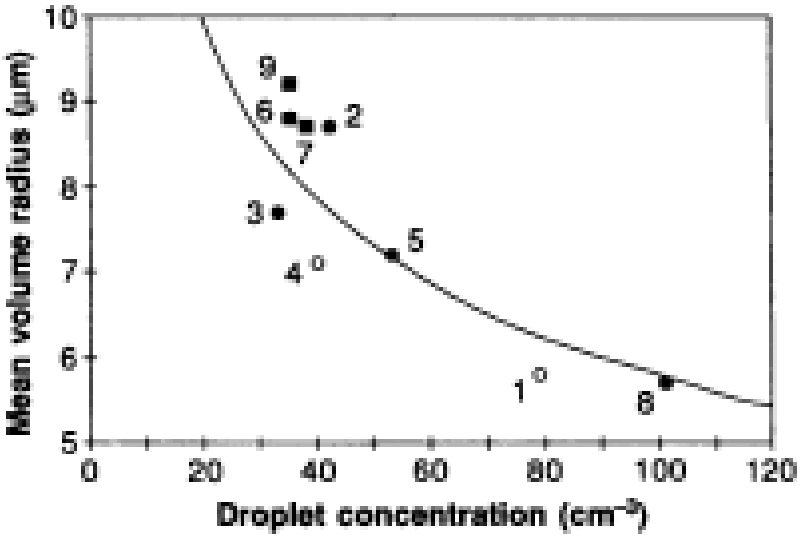

Figure 2.3: Albrecht (1989) figure showing the relationship between droplet concentration and mean volume radius produced from measurements obtained in horizontal homogeneous clouds ranging in depth from 150 m to 500 m in June and July of 1987 at 400 to 500 km southwest of Los Angeles, CA. The shaded circles and squares represent where drizzle and heavy drizzle was observed respectively.

3. Methodology

I. Biomass Burning Particle Identification

Since one of the primary objectives of this project is to identify the impacts of Central American biomass burning particles on convection in the Southern Great Plains, the most common biomass burning particle tracers in that region were identified. Southern Mexico and the Yucatan Peninsula were the regions from which biomass burning particles were most likely to come (Fig. 3.1). According to the Köppen climate classification system, most of the landscape in this region of focus is savanna. Most of the biomass burning taking place in Central America is performed to clear land for agricultural purposes (Wang et al. 2009). Echalar et al. (1995) investigated the biomass burning particles emitted from forest and savanna fires. It was found that the biomass burning particles emitted from the two landscapes were different. In all the savanna landscapes that Echalar et al. (1995) examined, a similar pattern was observed with all the biomass burning particles enriched in fine potassium, fine zinc, and bromine with organic carbon being the predominant chemical produced. The chemicals produced from savanna landscape were used as the predominant aerosol tracers of biomass burning in the Southern Great Plains. One limiting factor of this method, however, is that chemical characteristics of particles may be different if the emission is from a different vegetation source.

II. Savanna Biomass Burning Concentration Climatology, Storm Identification Days, and Bootstrapping Technique

Two sites in western Oklahoma were used to produce the savanna biomass burning particle (hereafter *biomass burning particle*) climatology (Fig. 3.2): Wichita Mountains (located in Comanche County, southwestern Oklahoma) and Ellis (located in Ellis County, northwest Oklahoma). The aerosol data were obtained from the Federal Land Manager Environmental Database (FED). Organic carbon, fine potassium, fine zinc, and bromine were the chemicals used to construct an eleven-year climatology (2002-2012) of the biomass burning particle concentrations. The aerosol data and particles species were collected using measurements from the Interagency Monitoring of Protected Visual Environments (IMPROVE). Fine bromine, potassium, and zinc measurements were taken using a special sampler used in the IMPROVE network, module A (IMPROVE, 2006). Organic carbon measurements were taken using another special sampler, module C (IMPROVE, 1995). An average concentration of each of the biomass burning particles in western Oklahoma was obtained for each of the days there were data (every three days) using both sites. Once prevalence of each of the biomass burning particles was identified for each day, days were classified into high (upper 30%), medium (middle 40%), and low (lowest 30%) biomass burning particle concentration for each of the particles. Days were only included in the 'high' category if at least 3 out of the 4 tracers were in the top 30%; only in the 'medium' category if at least 3 out of the 4 tracers were in the middle 40%; and only in the 'low' category if at least 3 out of the 4 tracers were in the lowest 30%.

Only March through June was considered since this is climatologically the convective season in the Southern Great Plains. It was found that there were 92 high biomass burning concentration days, 72 medium biomass burning concentration days, and 55 low biomass burning concentration days.

From the subset of days on which aerosol data were available, days when severe weather occurred in the study area (western Oklahoma Fig. 3.2) were identified. Hail and wind were the primary severe weather modes examined as they were more common. Storm reports were obtained from the National Climatic Data Center (NCDC), which records data on storms that produce reports of severe-criteria hail or wind. The NCDC database records the type of weather hazard (e.g., thunderstorm wind, hail, tornadoes) along with the intensity, time, and county of occurrence. In January 2010, the National Weather Service changed the severe hail size threshold from 0.75 to 1.00 inch, so 1.00 inch was used as the threshold for severe hail for all years considered for this climatology while a wind speed threshold of 50 kts was used for severe wind.

To provide evidence that a change in the distribution of hail size and wind speed may be a function of aerosol concentration, days with similar thermodynamic and kinematic environments were examined and chosen as case study days. The thermodynamic parameters chosen were surface-based convective available potential energy (CAPE) and 100 mb mixed-layer CAPE, which measures the mean CAPE available to air parcels in the lowest 100 mb. The kinematic parameter chosen was 0-6 km shear. The combination of CAPE and deep-layer shear aid in assessing updraft strength. Stronger updrafts contain higher supersaturation, leading to more rapid droplet growth. These parameters were

interpolated using archive maps obtained from the Storm Prediction Center (SPC) mesoanalysis. One limiting factor of this method is that storm type (e.g., supercell, multicell, squall line) is not taken into account though two different storm mode could develop in a similar thermodynamic and kinematic environment, the distribution of hail size and surface wind speed could vary between them. After performing this analysis, the number of days in which storm reports were examined between each aerosol concentration category was substantially reduced. There were 14 days in the high aerosol category, 10 days in the medium aerosol category, and 8 days in the low aerosol category.

As a result of the substantial reduction in the number of days analyzed for each aerosol concentration category, the sample hail size and wind speed were limited. To produce a large enough sample size from the available data, the bootstrapping technique was applied. This method was first introduced by Efron (1979) and has been widely used since. The idea behind bootstrapping is to take a sample of data, which in this case is hail size and wind speed values, and to randomly sample these values with replacement. To get a large enough sample size, the bootstrap was applied 1000 times to all the sample hail sizes and wind speeds in each aerosol category.

III. Synoptic Patterns and Parcel Trajectories during Days of Different Aerosol Concentration

Since it has been shown that certain synoptic patterns are more favorable than others for transport of biomass burning particles from Central America to the Southern Great

Plains (Wang et al. 2009), a detailed compositing of synoptic patterns near the surface was undertaken during all the days of the different aerosol concentrations. Mid-level tropospheric synoptic pattern composites (e.g. 500 hPa) were also obtained to aid in the explanation of the surface pattern.

To provide evidence that the high concentration of biomass burning particles seen on specific days in the Southern Great Plains originated from the known source region in Central America, air parcels on the different case study days obtained were tracked using the HYbrid Single-Particle Lagrangian Integrated Trajectory (HYSPLIT) model operated by the Air Resources Laboratory. This model incorporates the North American Regional Reanalysis (NARR) to compute forward and backward trajectories of air parcels at a given location and height for a given time. The trajectories display parcel position every 6 hours. The starting position incorporated into the model was 35°N latitude and 99°W longitude (Fig. 3.2), which is within the region of study. Air parcels were tracked at 100 m and 300 m above ground level to examine whether the trajectories observed were consistent with the synoptic pattern. A backward parcel trajectory up to 96 hours (4 days) was initialized within the model to examine where parcels originated, as it was a sufficient time period to analyze the source region.

IV. Polarmetric Radar Variables Used to Infer Thunderstorm Microphysics

Another primary objective of this study is to identify microphysical differences in thunderstorms between days of different aerosol concentration. Microphysical differences

between thunderstorms can be inferred using polarimetric radar data. Dual polarization radars emit and receive electromagnetic radiation with both horizontal and vertical polarization. As of 2013, most of the Weather Surveillance Radar-1988 Doppler (WSR-88D) radars around the U.S. had been upgraded to dual polarization capability.

A hypothesis from much prior research is that higher aerosol concentration produces smaller cloud droplets within developing clouds, delaying the warm rain process and aiding in convective invigoration. Two sets of case studies using polarimetric radar data will be examined to test if an altered drop size distribution (DSD) is seen. Due to the recent upgrade of polarimetric radar and only having aerosol data up to 2012, there are very few days of different aerosol concentration and storm occurrence. This limited the amount of cases to analyze. Two polarimetric variables that will be used to examine the storm microphysics between days of different aerosol concentration are differential reflectivity (Z_{DR}) and copolar cross-correlation coefficient (ρ_{hv}). Since S-band radar is not capable of examining cloud droplet size particles, raindrop particle size will need to be measured. With small cloud droplets, coalescence efficiency will be small and therefore it will take longer for a raindrop particle to grow to a larger size (Rosenfeld, 1999). As a result, cloud droplet size can be inferred by examining raindrop size. Z_{DR} is a measure comparing the horizontally-polarized return signal to the vertically-polarized return signal and is defined as:

$$Z_{DR} = 10\log_{10}(Z_h/Z_v) \quad (1)$$

where Z_h is the horizontal power return and Z_v is the vertical power return. Therefore, Z_{DR} gives an estimate of the oblateness of hydrometers in a given sample volume. Drop oblateness increases with increasing raindrop diameter (Beard et al. 1989). ρ_{hv} is a measure of the correlation between the horizontally and vertically returned power signals and is defined as:

$$\rho_{hv} = \frac{\langle S_{hh} S_{vv}^{*} \rangle}{\sqrt{|S_{hh}|^2 |S_{vv}|^2}} \quad (2)$$

where S_{hh} is the amplitude of the co-polarized pulse in the horizontal and S_{vv} is the amplitude of the co-polarized pulse in the vertical within a sample volume; the first and second subscripts respectively identify the polarization of the backscattered and incident fields. Therefore, ρ_{hv} can be useful for identifying whether there is a uniform DSD or if there is a mixture of droplet sizes or particle phases within a given sample volume. ρ_{hv} can provide additional insight, along with $Z_{DR,}$ of the hydrometer size distribution within a sample volume. Since high CCN concentration results in small drops, a clear polarimetric signature should be evident. High CCN concentration should result in Z_{DR} values between 0-1 dB and ρ_{hv} values close to 1 (Straka et al. 2000).

The first two cases examined were thunderstorms in the High Plains region near the Cheyenne, Wyoming radar (KCYS) on 15 June and 21 June 2013. 21 June was a high aerosol day compared to 15 June. The other cases examined were thunderstorms on 24 May 2011 in the range of the Vance Air Force Base radar (KVNX) in northwestern Oklahoma and 10 May 2010 near the Norman, Oklahoma radar (KOUN). 24 May 2011 was a high aerosol day compared to 10 May, 2010. The aerosol data were obtained from

the Environmental Protection Agency (EPA). PM2.5 and PM10 were the particulates used to measure the aerosol concentration on each of the case study days.

Figure 3.1: The region of Central America favored for biomass burning particles origination.

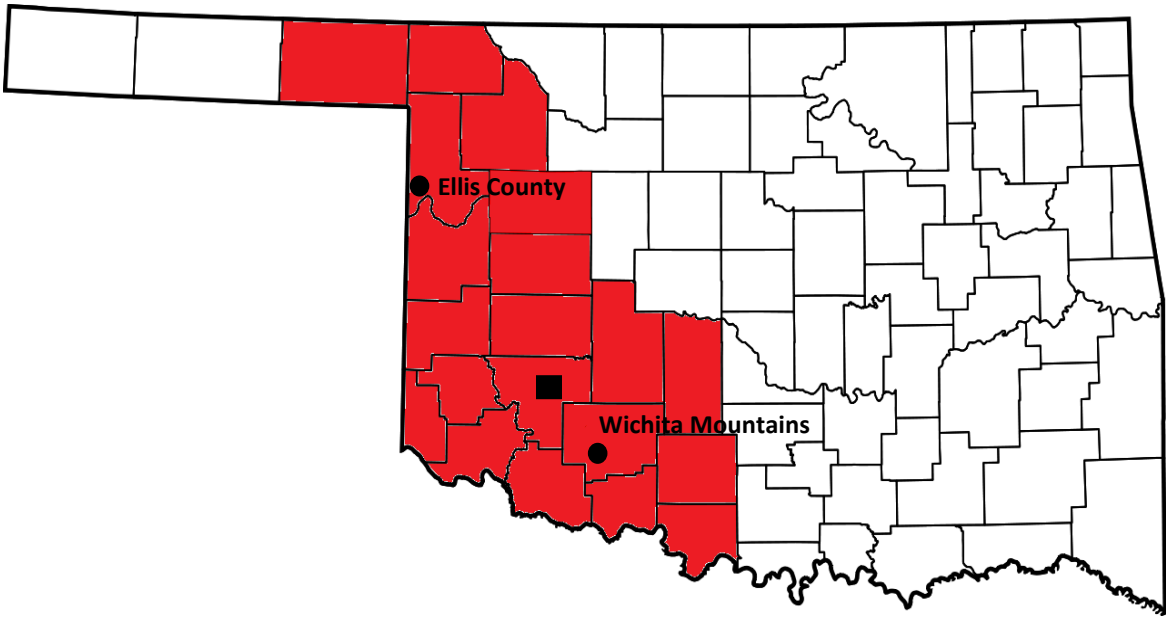

Figure 3.2: Area of study (red shaded counties in western OK) with Ellis County and Wichita Mountains representing sites from which aerosol data were obtained. The square represents the approximate start location of the backward parcel trajectory using the HYSPLIT model.

4. Distribution of Hail Size and Surface Wind Speed as a Function of Aerosol Concentration

The hail and surface wind speed reports from the region of study in western Oklahoma were compared for the different aerosol concentration categories to examine if a trend was apparent. Figures 4.1a and 4.1b show the distribution of hail size and surface wind speed respectively from the severe weather reports, using the NCDC data source for several aerosol concentration categories after applying the bootstrapping technique. It was found that the distribution shifts towards larger hail size and higher wind speeds with higher aerosol concentration. This was a statistically significant ($p<0.001$) result, suggesting that aerosols may have played a role in altering the storm microphysics, possibly increasing updraft and downdraft strength.

Many have hypothesized that greater aerosol concentration leads to smaller cloud droplets, delaying the warm rain process and allowing more cloud water to be transported vertically to form a higher number concentration of liquid droplets and ice crystals aloft (Rosenfeld 1999; Andreae et al. 2004; Lin et al. 2006; Yuan et al. 2011; Rosenfeld and Bell 2011). With a higher number concentration of liquid droplets and ice crystals aloft, latent heat release and updraft strength are enhanced. This enhancement of the updraft may explain why larger hail size was more common with higher aerosol concentration. Since there is also greater sublimation of ice and evaporation of droplets given a non-saturated environment, downdraft strength is also increased (Khain et al. 2005). This

increase in the downdraft strength may explain why stronger surface winds were more common with higher aerosol concentration.

Even though the case study days were chosen based on similar thermodynamic and kinematic environments, this does not take into account storm type (e.g., supercell, multicell, and squall line). As mentioned, storm type could have a significant influence on the behavior of hail size and surface wind speed. The number of storm reports was limited by the limited number of days for each aerosol concentration category. Even though the bootstrap technique was applied to reduce the impact of limited data, inclusion of additional storm reports would lead to a more robust result.

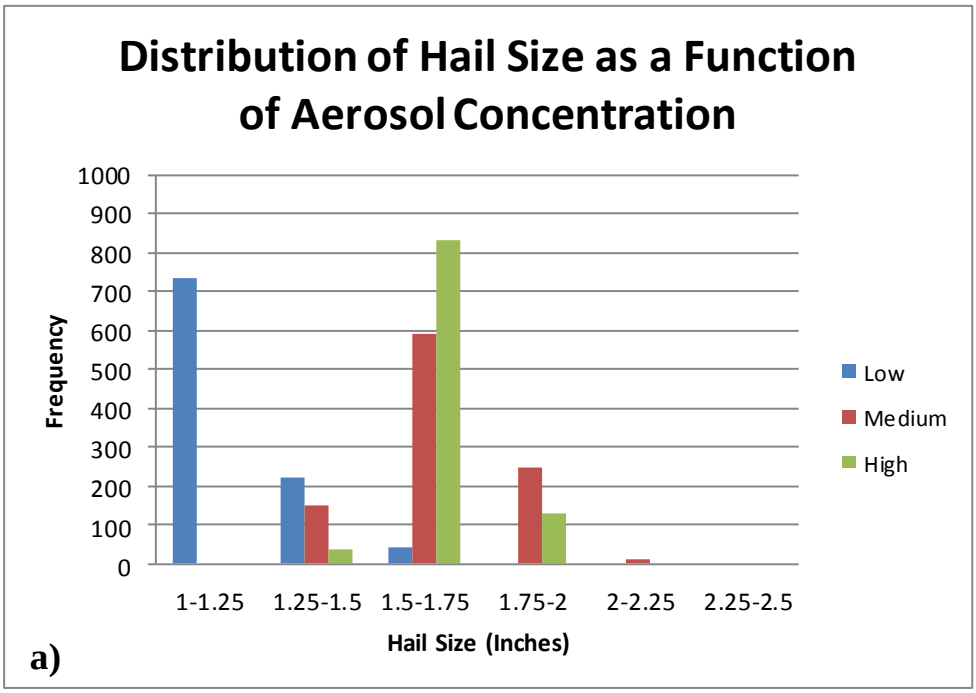

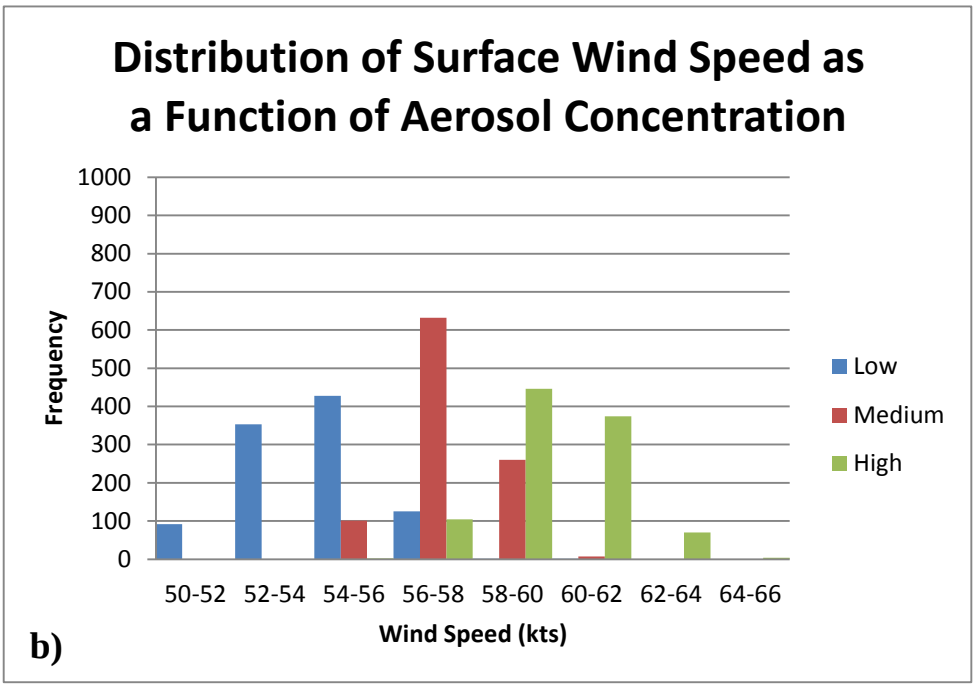

Figure 4.1: Distribution of (a) hail size and (b) surface wind speed using bootstrapping technique. Low, medium, and high denote aerosol concentration, as defined in the Methodology.

5. Synoptic Regimes and Parcel Path Trajectories during Different Aerosol Concentration Categories

a) Synoptic Regimes during Different Aerosol Concentration Categories

The composite surface and 500 hPa flow patterns were analyzed for all high, medium, and low aerosol concentration days. Examining the sea-level pressure map for low aerosol days, the area of lowest pressure was located in southern Illinois (Fig. 5.1a). This allowed the flow in the Central Plains to be northerly (Fig. 5.2a). The position of the surface pressure pattern, however, significantly changed for medium aerosol days. The area of lowest pressure was farther west, extending from the central to southern High Plains (Fig. 5.1b). This configuration allowed the flow to be southerly (Fig. 5.2b), resulting in flow originating more from the western Gulf of Mexico and Yucatan Peninsula region. This pattern would be conducive for greater transport of biomass burning particles from the Yucatan Peninsula into the Southern Plains, especially within the planetary boundary layer (e.g., Wang et al. 2009). The same configuration was observed with high aerosol days, with the area of lowest pressure confined to the southern High Plains. Lower pressures, however, were observed during high aerosol days as the composite surface pressure was approximately 2-3 hPa lower compared to medium aerosol days (Fig. 5.1c). This produced a difference in the surface wind flow configuration between medium and high aerosol days. Even though the composite wind speed was similar (5-7 ms^{-1}), the distribution of the wind speed was different. During medium aerosol days, the maximum in the composite surface wind speed was confined to

the western Gulf of Mexico into southern Texas (Fig. 5.2b). During high aerosol days, the maximum in the composite surface wind speed extended farther north into southwestern Oklahoma (Fig. 5.2c). The stronger flow extending farther north would be more conducive for flow originating from the western Gulf of Mexico and the Yucatan Peninsula to be advected farther north.

The composite sea-level pressure pattern observed during the different aerosol concentration days can be attributed to the synoptic regime at 500 hPa. During low aerosol days, the 500 hPa trough axis was located from the Central Plains into the Midwest (Fig 5.3a). This forced the location of the surface cyclone to be farther east into Illinois, therefore forcing the surface flow to be northerly across most of the Central Plains. During medium and high aerosol days, however, the 500 hPa trough axis was located farther west into California and Nevada (Fig. 5.3b-c). This forced the surface cyclone to be located farther west over the central and southern High Plains. The 500 hPa composite wind flow was stronger on high aerosol days compared to medium aerosol days (Fig. 5.4b-c). The stronger flow was most likely a result of the greater amplitude of the height pattern (Fig. 5.3c). The stronger flow observed at 500 hPa may partially explain the stronger surface cyclone observed during high aerosol days compared to medium aerosol days due to possibly stronger divergence created.

b) *Parcel Path Trajectories Common During Different Aerosol Concentration Categories*

Using the HYSPLIT model, backward parcel trajectories at 2 and 4 days prior to the aerosol observation day were performed to examine origin regions (Fig. 5.5). During low aerosol days there was a significant clustering of parcels in the north region at 2 days prior (Fig 5.6a). On approximately 34% of days, parcels originated from this region (Table 5.1). This occurred at both 100 m and 300 m. At 4 days prior to a low aerosol day, there was not a clear region as to where parcels were clustered (Fig 5.6b). This may have occurred as parcels at 100 m and 300 m were farther separated from each other. Despite the lack of clustering, on approximately 41% and 37% of days parcels at 100 m and 300 m respectively originated from the north region (Table 5.1). This was consistent with the observed composite surface wind flow during low aerosol days as the flow was northerly.

During medium aerosol days, there were noticeable differences in the parcel location compared to low aerosol days (Fig. 5.7). At 2 days prior, there was a significant clustering of parcels in the western Gulf of Mexico region (Fig. 5.7a). On approximately 34% of the medium aerosol days parcels at 100 m originated from this region (Table 5.1). This is consistent with the observed composite surface wind flow during medium aerosol days as the flow was southerly. At 4 days prior, there was not a clear region as to where parcels originated as a result of the greater separation of parcels at 100 m and 300 m (Fig. 5.7b). Despite the lack of clustering, on approximately 33% of the days at both the 100 m and 300 m levels, parcels originated from the north region (Table 5.1).

During high aerosol days, there was a more noticeable clustering of parcel origination points at both 2 and 4 days prior. At 2 days prior, there was a significant clustering of parcels in the western Gulf of Mexico region (Fig 5.8a). On approximately 30% of days, parcels originated from this region at both 100 m and 300 m (Table 5.1). At 4 days prior, a significant clustering of parcels was still evident in the western Gulf of Mexico region (Fig. 5.8b), with a higher percentages of parcels originating from the Yucatan Peninsula/western Caribbean region (Table 5.1). These observed trajectories at 2 to 4 days prior at both 100 m and 300 m is consistent with the observed composite southerly wind flow.

When comparing the parcel path trajectories between each of the different aerosol concentration categories, it is evident that there are more instances in which parcels originate from the north region during low aerosol days while originating from the western Gulf of Mexico region during medium and high aerosol days. This is consistent with the composite surface wind flow pattern observed for all three concentration categories. Even though there are more cases in which parcels originate from the Yucatan Peninsula/western Caribbean region during high aerosol days, this does not represent a high percentage of days in this category. Even though wildfires can occur in other regions, the biomass burning characteristics were identified based on the savanna landscape that composes most of southern Mexico and the Yucatan Peninsula, making this a limitation of this study. A complicating factor was the parcel path trajectories during the days prior to the aerosol observation days were both ascending and descending to different height levels. The wind direction could vary at these different height levels

that parcels traversed, significantly influencing path trajectories. Another complicating factor was that even though the 100 m and 300 m levels are very close to each other, the parcels at each level were more widely separated at 4 days prior to the aerosol observation day. This raises uncertainty in the path trajectories the farther in time backward trajectories are performed.

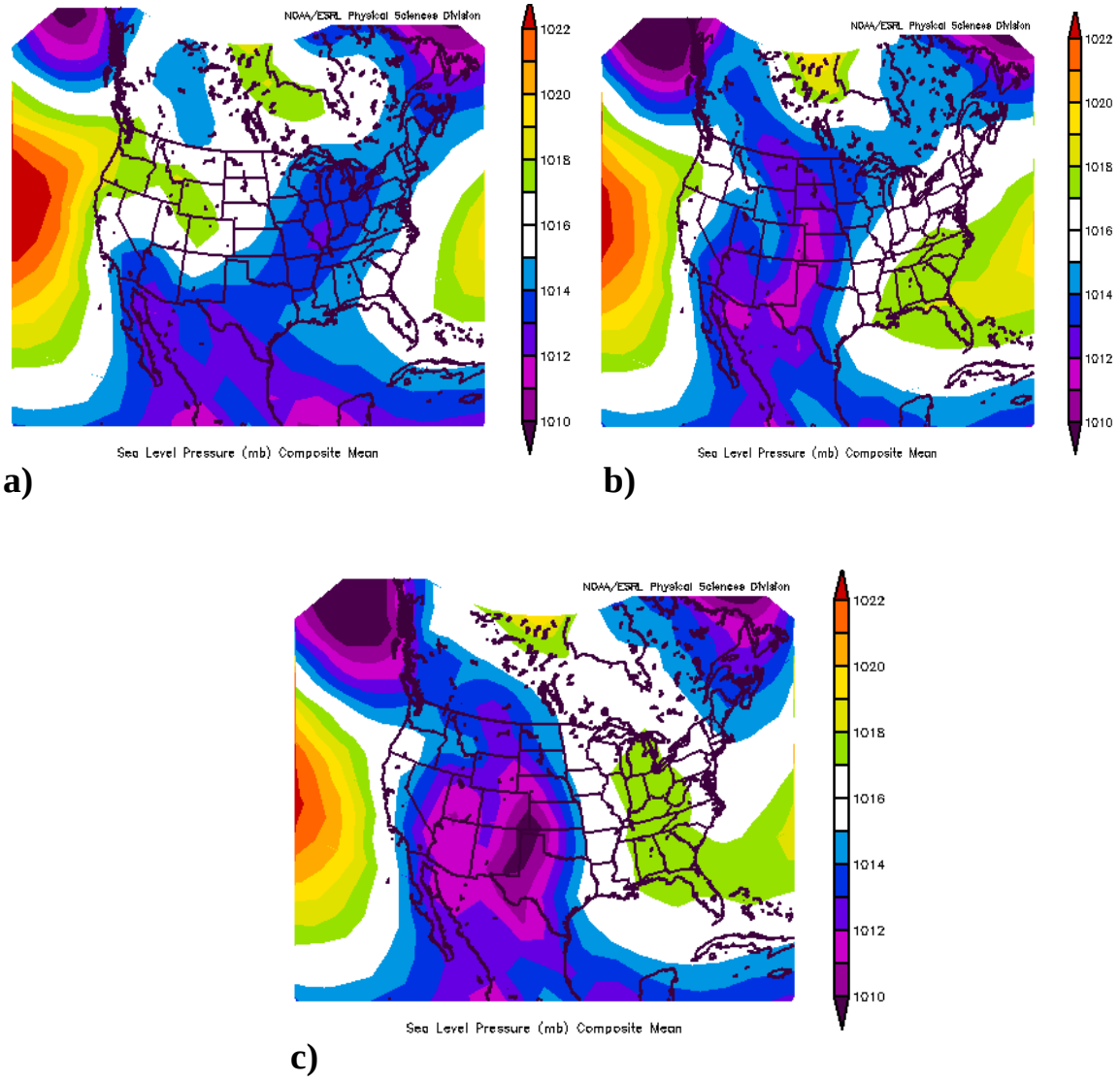

Figure 5.1: Sea-level surface composite for all: a) low aerosol days, b) medium aerosol days, and c) high aerosol days. The color fill represents sea-level pressure in hPa.

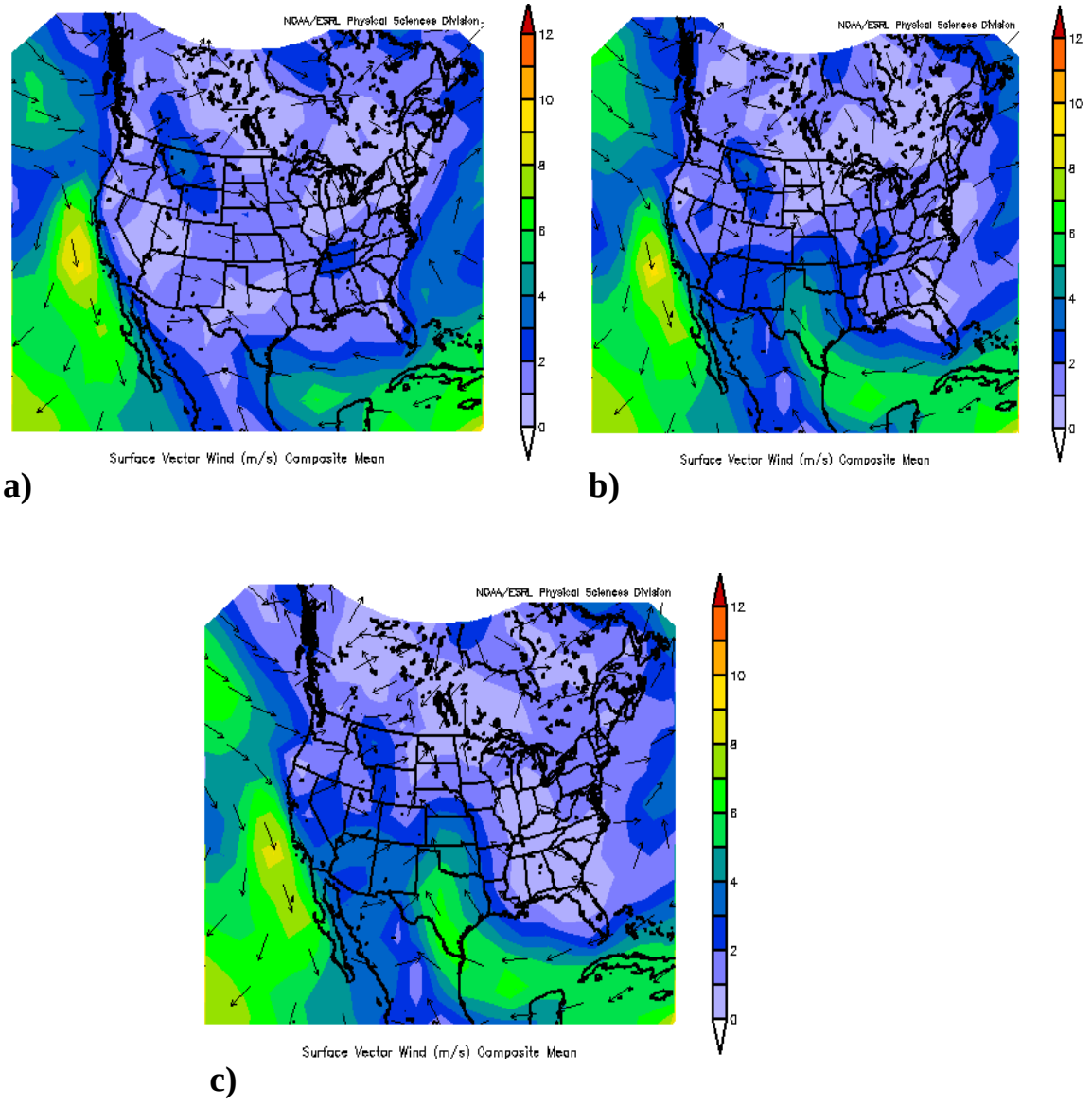

Figure 5.2: Surface wind flow composite for all: a) low aerosol days, b) medium aerosol days, and c) high aerosol days. The color fill represents wind speed in ms^{-1}.

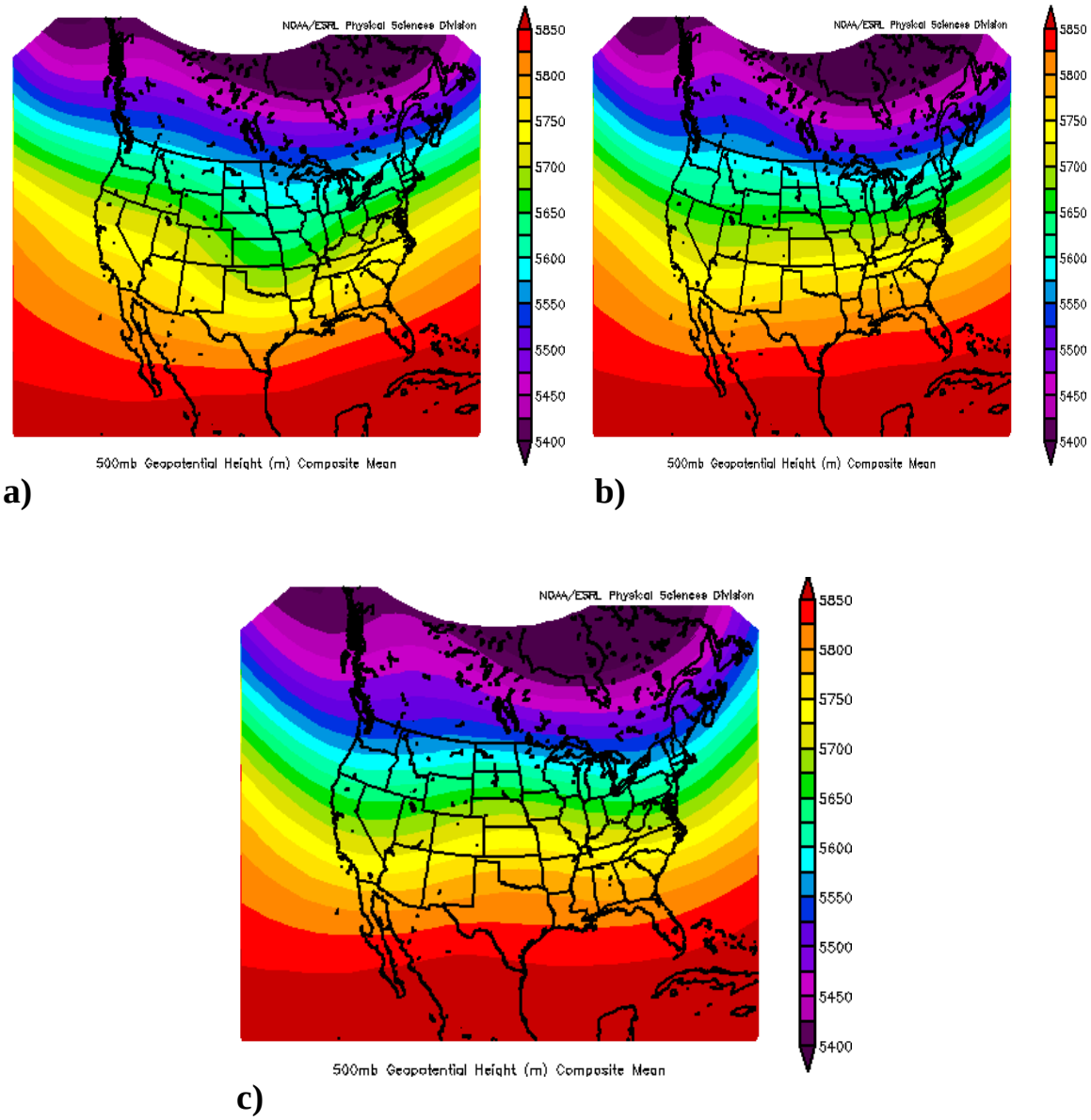

Figure 5.3: 500 hPa geopotential height composite for all: a) low aerosol days, b) medium aerosol days, and c) high aerosol days. The color fill represent geopotential height in meters.

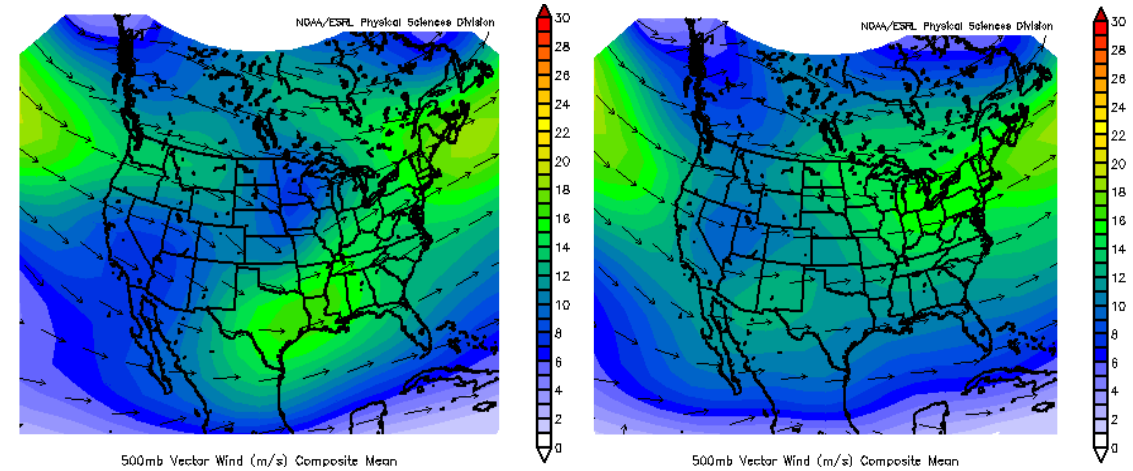

a) **b)**

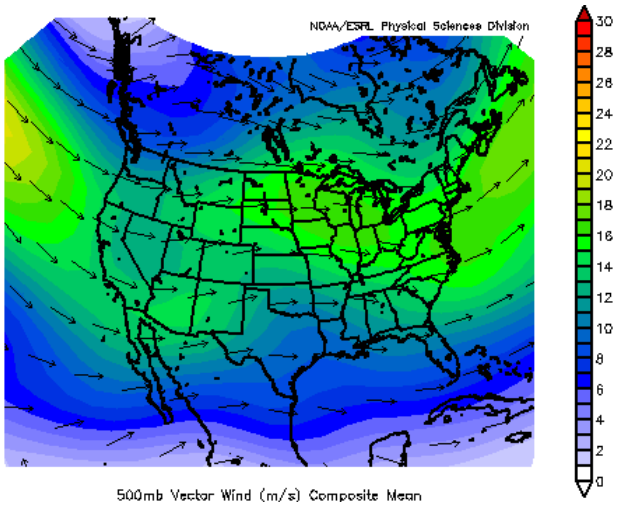

c)

Figure 5.4: 500 hPa wind flow composite for all: a) low aerosol days, b) medium aerosol days, and c) high aerosol days. The color fill represents wind speed in ms^{-1}.

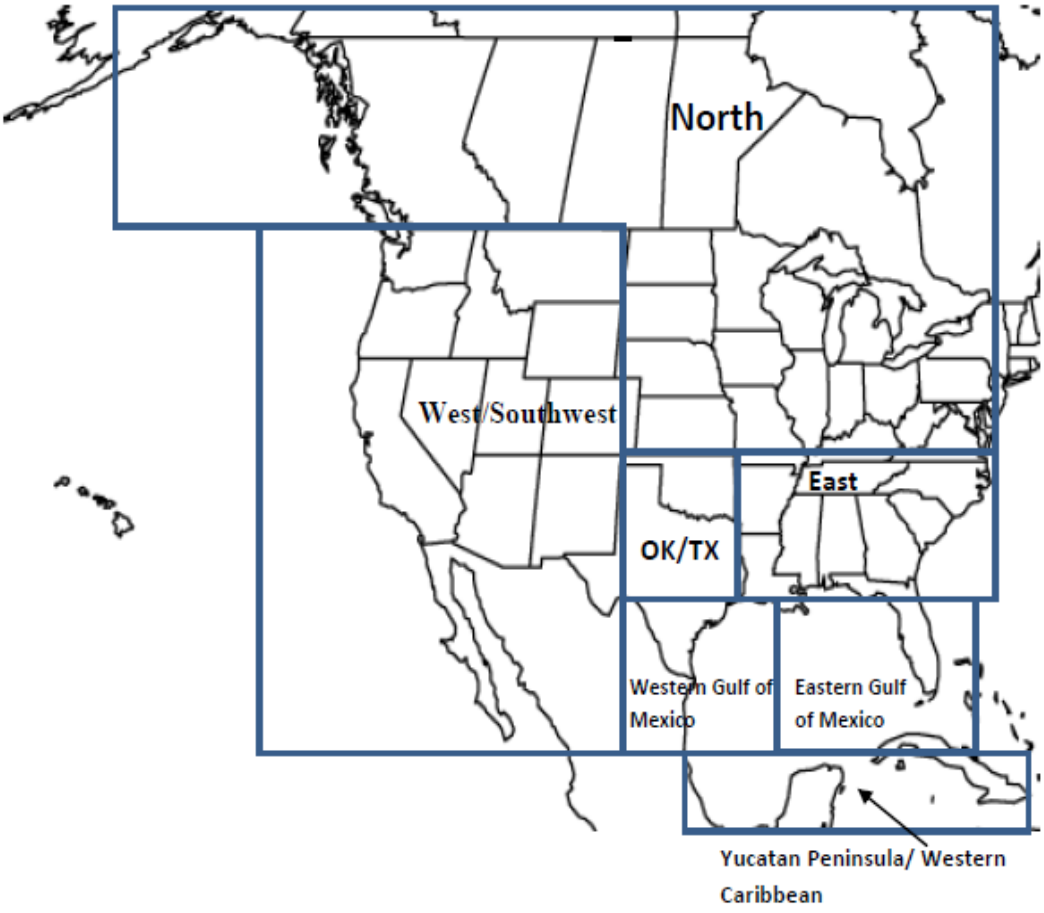

Figure 5.5: Parcel path trajectory location regions

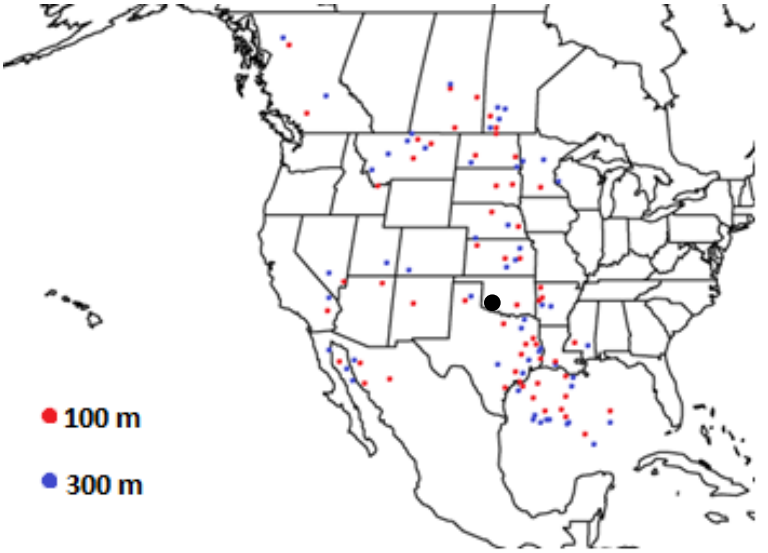

a)

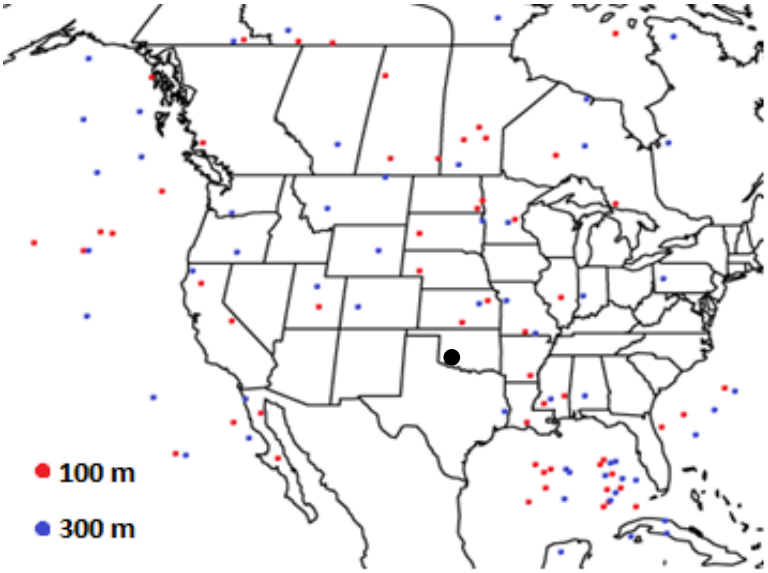

b)

Figure 5.6: Locations of parcels along backward trajectories at 100 m and 300 m for all low aerosol days at: a) 2 days prior and b) 4 days prior to the observation day. The black dot denotes the location at which the backward trajectory was initialized.

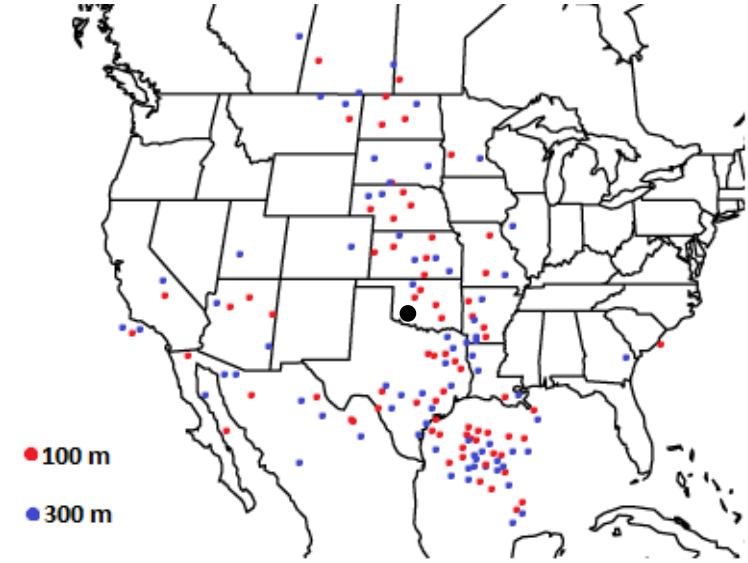

a)

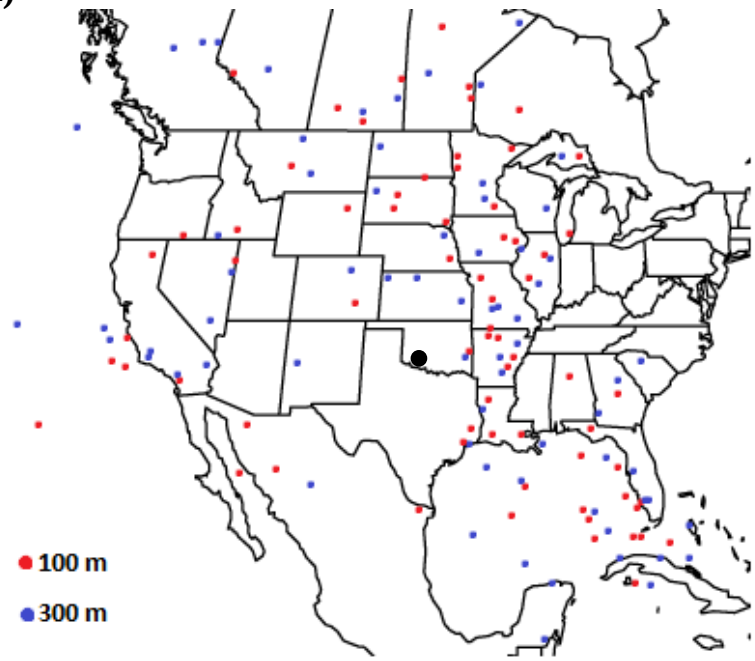

b)

Figure 5.7: As in Figure 5.6, except for all medium aerosol days.

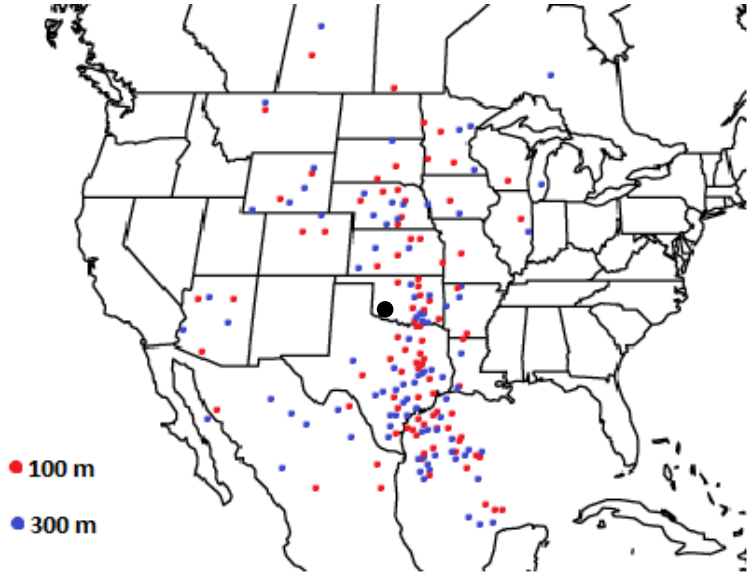

a)

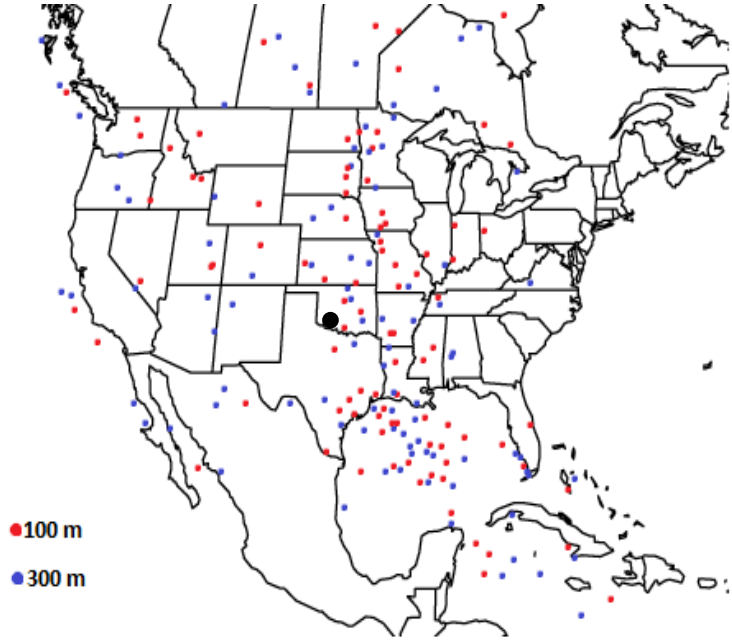

b)

Figure 5.8: As in Figure 5.7, except for all high aerosol days.

Average parcel location on low aerosol days

2 days	North	West and Southwest	OK and TX	East	Western Gulf of Mexico	Eastern Gulf of Mexico	Yucatan Peninsula and Western Caribbean
100 m	34%	21%	15%	4%	22%	4%	0%
300 m	34%	24%	13%	2%	20%	7%	0%
4 days	North	West and Southwest	OK and TX	East	Western Gulf of Mexico	Eastern Gulf of Mexico	Yucatan Peninsula and Western Caribbean
100 m	41%	22%	0%	9%	4%	24%	0%
300 m	37%	27%	2%	7%	0%	22%	5%

Average parcel location on medium aerosol days

2 days	North	West and Southwest	OK and TX	East	Western Gulf of Mexico	Eastern Gulf of Mexico	Yucatan Peninsula and Western Caribbean
100 m	22%	14%	17%	8%	34%	4%	1%
300 m	22%	22%	7%	17%	25%	4%	3%
4 days	North	West and Southwest	OK and TX	East	Western Gulf of Mexico	Eastern Gulf of Mexico	Yucatan Peninsula and Western Caribbean
100 m	33%	19%	3%	19%	8%	17%	1%
300 m	33%	26%	1%	11%	6%	17%	6%

Average parcel location on high aerosol days

2 days	North	West and Southwest	OK and TX	East	Western Gulf of Mexico	Eastern Gulf of Mexico	Yucatan Peninsula and Western Caribbean
100 m	25%	11%	25%	3%	33%	0%	3%
300 m	24%	15%	16%	6%	36%	0%	3%
4 days	North	West and Southwest	OK and TX	East	Western Gulf of Mexico	Eastern Gulf of Mexico	Yucatan Peninsula and Western Caribbean
100 m	33%	17%	4%	8%	17%	14%	7%
300 m	28%	22%	5%	10%	14%	13%	8%

Table 5.1: Average parcel locations (percentage) during low, medium, and high aerosol days at 100 m and 300 m above ground level at 2 and 4 days prior. The highlighted cells denote where parcel location at a particular level was >10% difference from the other locations.

6. Microphysical Differences in Thunderstorms from Days with Different Aerosol Concentrations

a) June 15th vs June 21st, 2013 High Plains Case Study Days

Figures 6.1a and 6.2b show the concentration of particulate matter of 2.5 micrometers in diameter or less (PM2.5) and particulate matter of 10 micrometers in diameter or less (PM10) respectively for Laramie County, Wyoming, for 15 and 21 June, 2013. Based on the figures, 21 June had approximately a 50% increase in PM2.5 concentration and approximately a 175% increase in PM10 concentration compared to 15 June. This suggests that higher CCN concentration was present on 21 June (Twomey 1974). The 300 mb flow over the region of convection on 15 June was southwesterly at approximately 55 kts and southwesterly between 50-60 kts on 21 June (Fig. 6.2). Both days had 500 mb winds from the southwest at approximately 30-40 kts (Fig. 6.3). The 0-6 km shear was around 50 kts on 15 June and between 40-50 kts on 21 June (Fig. 6.4). The main difference between the two days was the thermodynamic environment. The mixed-layer CAPE (MLCAPE) on 15 June was between 1000-1500 Jkg^{-1} while on 21 June it was between 2000-3000 Jkg^{-1} (Fig. 6.5). In an environment with higher instability updraft strength will be greater and depending on the vapor field within the updraft, a faster development of larger drops could occur. This should result in higher Z_{DR} values. Given that 21 June 2013 had a higher CCN concentration, it is possible that the higher CAPE could mask some of the hypothesized signal in the drop size.

Figure 6.6a shows the radar reflectivity image at 2001 UTC on 21 June. At this time a thunderstorm was developing just east of the Nebraska-Wyoming border. According to the vertical cross section of reflectivity, reflectivity values barely reached 30 dBZ anywhere in the developing storm (Fig. 6.6b). The vertical cross-section of differential reflectivity (Z_{DR}) shows that most of the developing storm had Z_{DR} values between 0 and 1 dB, indicating that small droplets were dominant at this time (Straka et al. 2000) (Fig. 6.6c). The vertical cross-section of correlation coefficient (ρ_{hv}) shows that most of the developing cloud had ρ_{hv} values close to 1, indicating a uniform droplet size distribution (Straka et al. 2000) (Fig. 6.6d).

At 2020 UTC, the thunderstorm continued to intensify as reflectivity values were approaching 40 dBZ (Fig. 6.7a-b). Examining the vertical cross section of Z_{DR}, values remained between 0 and 1 dB through most of the lower levels of the cloud, indicating that mostly small liquid droplets were present (Fig. 6.7c). This slowed collision coalescence process and therefore delayed the formation of larger droplets. The vertical cross-section of correlation coefficient shows that ρ_{hv} values were close to 1, indicating a continued uniform droplet size distribution (Fig. 6.7d).

On 15 June, characterized by a lower aerosol concentration, there were differences in the polarimetric radar data compared to 21 June. At 2150 UTC, a thunderstorm was developing northwest of Cheyenne, Wyoming, with reflectivity values over 40 dBZ (Fig. 6.8a-b). A vertical cross-section of Z_{DR} shows that unlike the 21 June storm in which Z_{DR} values were low (0-1 dB), there were higher Z_{DR} values (greater than 1 dB; Fig. 6.8c) at the same height level of 1500 m (solid line in Fig 6.7c and Fig. 6.8c). Z_{DR} was collocated

with reflectivity values greater than 40 dBZ and ρ_{hv} values near one (Fig. 6.8d), indicating that larger droplets were present during the developing stages of the storm (Straka et al. 2000).

At 2220 UTC reflectivity values were over 50 dBZ, especially along the western sector of the west-east vertical cross-section of reflectivity (Fig. 6.9b). At this point, small hail may have been falling along the same location, as there was a collocation of over 50 dBZ with low Z_{DR} values of 0-1 dB and ρ_{hv} values slightly below 0.98 (Fig. 6.9c-d). Along the eastern edge of the cross-section, there were locations where Z_{DR} values were above 2 dB. When this was collocated with reflectivity values over 40 dBZ and ρ_{hv} values near 1, larger droplets were indicated.

b) May 10th 2010 vs. May 24th 2011 Western Oklahoma Case Study Days

Figures 6.10a and 6.10b show the PM2.5 and PM10 concentrations respectively for Caddo County, Oklahoma for 10 May 2010 and 24 May 2011. Caddo County, OK was the site chosen to measure these particle concentrations as storms occurred near this location on days. According to the figures, 24 May 2011 had approximately a 230% increase in PM2.5 concentration and approximately a 150% increase in PM10 concentration compared to 10 May 2010. The 300 mb flow over the region of convection on 10 May 2010 and 24 May 2011 was from the southwest between 70-80 kts and around 70 kts respectively (Fig. 6.11). At 500 mb, a strong trough was affecting the Central Plains on both days with 70 kts of west-southwest flow on 10 May 2010 and 50 kts of

southwest flow on 24 May 2011 (Fig. 6.12). The 0-6 km bulk shear on 10 May 2010 was between 70-80 kts while on 24 May 2011 it was between 40-50 kts (Fig. 6.13). The thermodynamic environment was similar as the MLCAPE on 24 May 2011 was approximately 4000 Jkg^{-1} while on 10 May 2010 it was approximately 3000 Jkg^{-1} (Fig. 6.14). In the stronger sheared environment, the updraft strength will be stronger as it is tilted farther away from the region of precipitation loading. Depending on the vapor field within the updraft, faster development of larger drops could occur, resulting in higher Z_{DR} values. Though the shear was stronger on 10 May, the limited number of dual-pol cases precludes obtaining a more similar comparison.

Figure 6.15a shows the radar reflectivity image of a thunderstorm developing in Custer County, OK at 1852 UTC on 24 May 2011. The vertical cross-section of reflectivity shows reflectivity values mostly over 40 dBZ with some areas over 50 dBZ (Fig. 6.15b). Examining the vertical cross-section of differential reflectivity, most of the lower levels of the developing storm had Z_{DR} values of 0 to 1 dB (Fig. 6.15c). Collocated with the low Z_{DR} values were ρ_{hv} values near 1 (Fig. 6.15d). There is, however, a corridor of high Z_{DR} values (greater than 3 dB) associated with the developing updraft. At this early stage of the storm lifecycle, most of the cloud is composed of updrafts. Surrounding the main updraft are weaker updrafts, which will have lower supersaturation. This will produce a smaller droplet growth rate. Prior studies have looked at all portions of the developing convection with reflectivity values >20 dBZ, not just the strongest updraft region, to access the DSD (May et al. 2011). The surrounding weaker updrafts along with the low Z_{DR} values and high ρ_{hv} values were indications that locations surrounding the

main updraft had a high concentration of small droplets at this stage of the storm life cycle.

10 May 2010, as mentioned, had lower aerosol concentration compared to 24 May 2011. There were also microphysical differences in the storms that developed this day compared to 24 May 2011. Figure 6.16a shows the radar reflectivity image of a developing thunderstorm in Grady County, Oklahoma at 2250 UTC at approximately 1.5 km above ground level. Reflectivity values were over 50 dBZ along the northwest flank. Along the same location, Z_{DR} values were over 3 dB and ρ_{hv} values were near 1 (Fig. 6.16b and Fig. 6.16c). Unlike the 24 May 2011 case when there was a small area of Z_{DR} values over 3 dB, the 10 May 2010 storm had a significantly larger area of Z_{DR} values over 3 dB. This suggests that larger droplets were predominant through most of the lower levels of the storm.

Both High Plains and Oklahoma case studies exhibited the same polarimetric radar patterns. On 21 June 2013 (High Plains case study day) and 24 May 2011 (Oklahoma case study day), small droplets were evident through most of the storm's lifecycle. On 15 June 2013 (High Plains case study day) and 10 May 2010 (Oklahoma case study day), larger droplets were more evident through most of the storm's lifecycle. Both 21 June 2013 and 24 May 2011 were days with higher aerosol concentration compared to 15 June 2013 and 10 May 2010. Smaller droplets being more evident on the high aerosol days is indicative that small cloud droplets were present. This is consistent with the findings of Rosenfeld (1999) and May et al. (2011) of smoke-filled clouds having a higher concentration of smaller droplets. On 21 June 2013, the first radar echoes appeared with

cloud top height at approximately 10.5 km while on 15 June 2013 the first radar echoes appeared with a lower cloud top height, approximately 9 km. This is consistent with the findings of Battan and Braham (1956) in that the radar echoes first appeared in a low CCN environment with tops as low as 2000 m, whereas radar echoes first appeared in a higher CCN environment with substantially higher cloud tops.

The differences observed in the polarimetric data when comparing days with different aerosol concentration suggest that aerosols may have played an important role in altering storm microphysics, however, the effects may have been more noticeable during the High Plains cases than the Oklahoma cases due to differing environmental parameters. The High Plains cases had similar shear, but different MLCAPE. 21 June 2013 (the high aerosol day) had higher instability compared to 15 June 2013, suggesting a stronger updraft was present. 21 June 2013 had higher dewpoints, 13-15°C, compared to 7°C on 15 June 2013. The combination of higher dewpoints and stronger updrafts would suggest a faster development of larger drops should have occurred on 21 June 2013. This effect, however, was not observed through most of the developing stages of the storm lifecycle as small droplets were predominant due to low Z_{DR} values. This suggests of a significant aerosol effect on 21 June 2013. Even though smaller droplets were observed on 24 May 2011 compared to 10 May 2010, suggestive of an aerosol effect, the kinematic environment was significantly different. The kinematic environment could have had a more significant impact than aerosols did in altering the storm microphysics as a result of the updraft strength being altered, which could affect the development rate of larger drops. This uncertainty presents a limitation of the polarimetric analysis due to the very

limited number of cases available as a result of the recent upgrade to polarimetric capability on all WSR-88D radars.

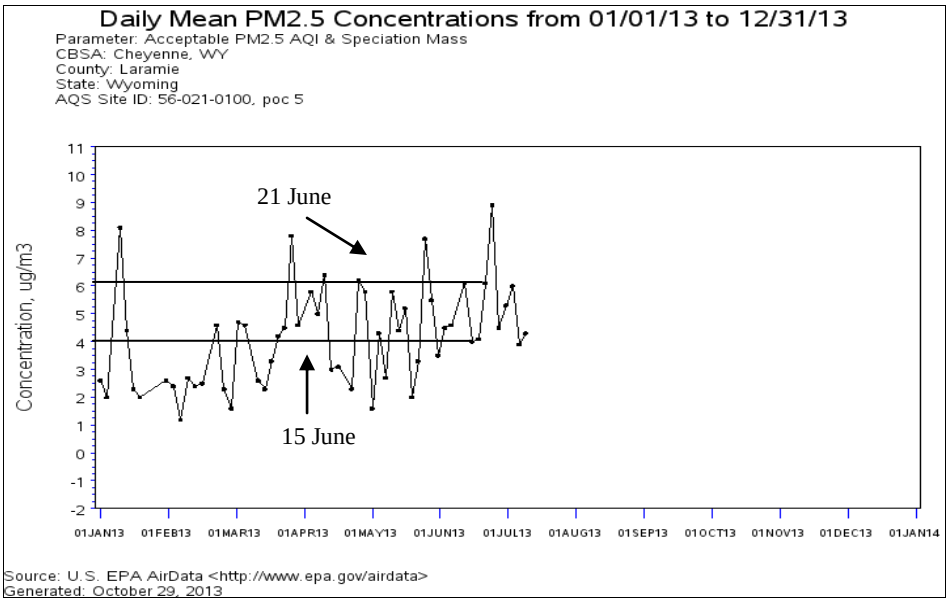

a)

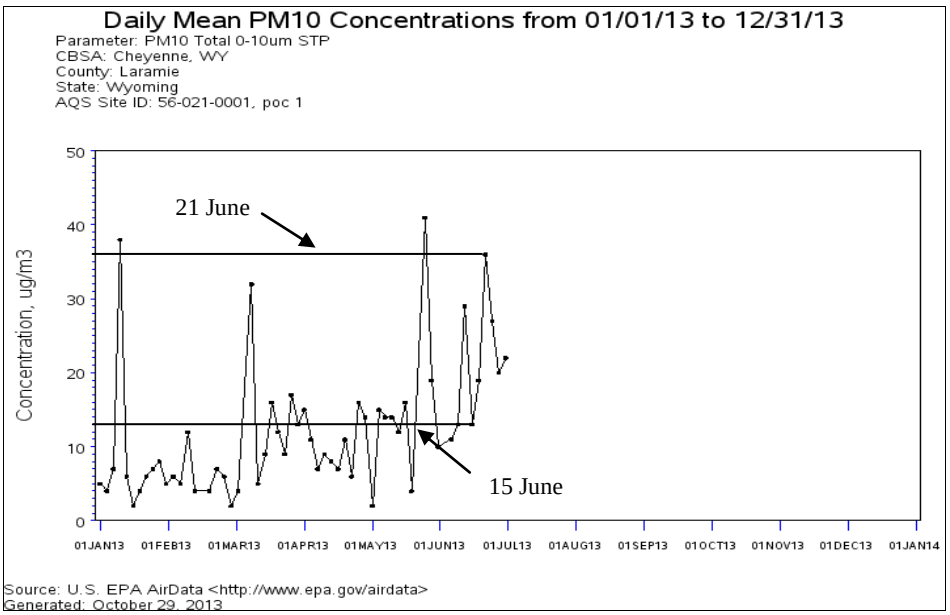

b)

Figure 6.1: a) PM2.5 concentration for Laramie County, WY for 15 June and 21 June 2013 and b) PM10 concentration for Laramie Country, WY, for 15 June and 21 June 2013

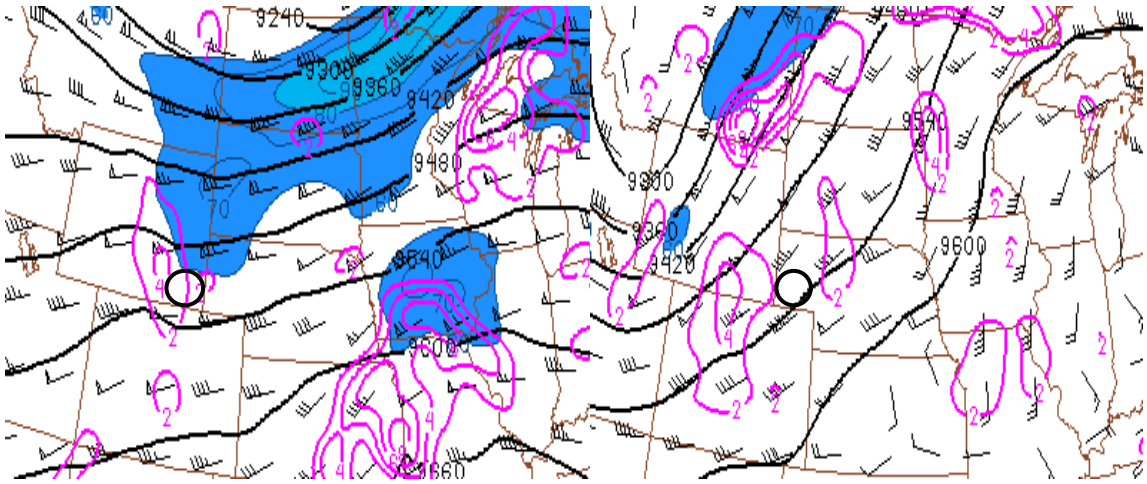

a) **b)**

Figure 6.2: 300 mb flow for- a) 15 June and b) 21 June. The oval indicates the approximate location storms developed on each day.

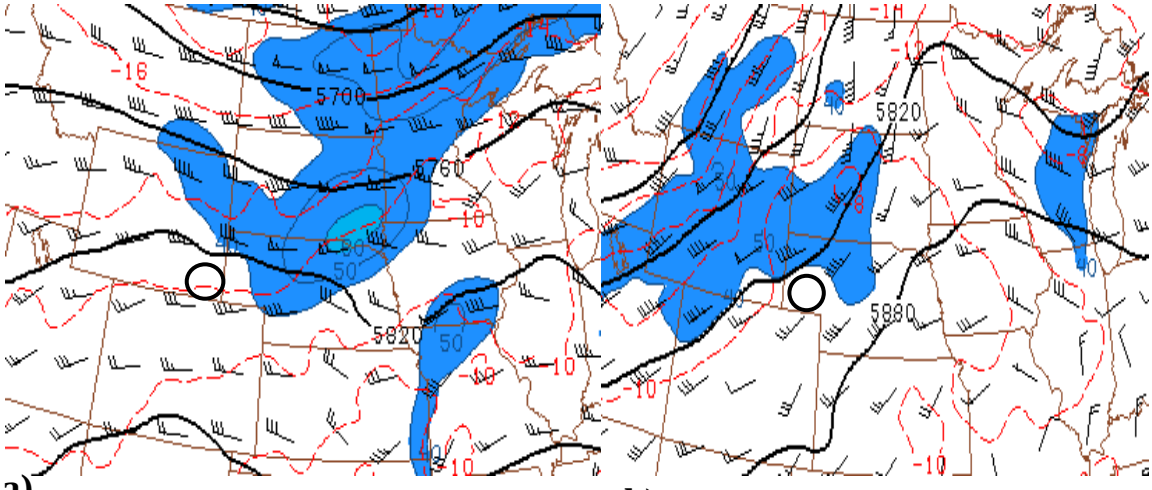

a) **b)**

Figure 6.3: As in figure 6.2, except for the 500 mb flow

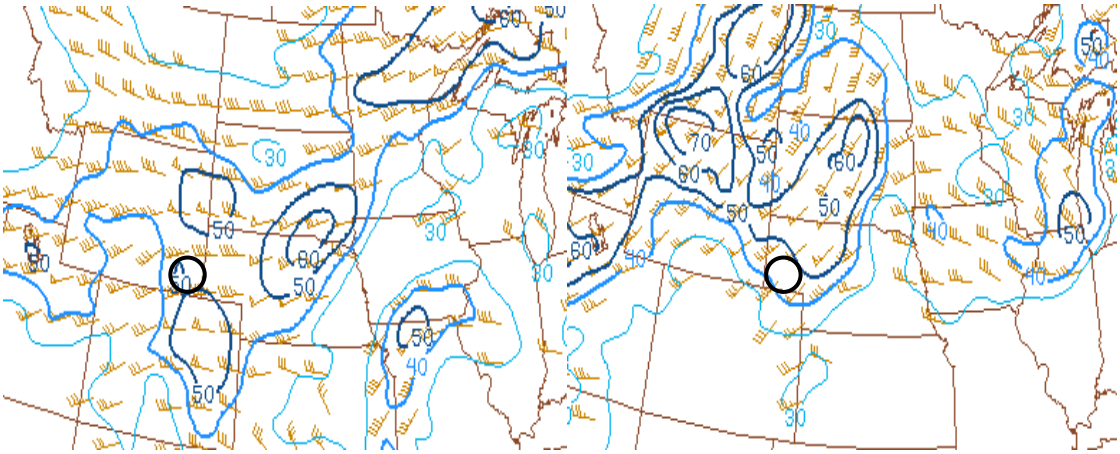

a) **b)**

Figure 6.4: 0-6 km bulk shear for- a) 15 June and b) 21 June. The oval indicates the approximate location storms developed on each day.

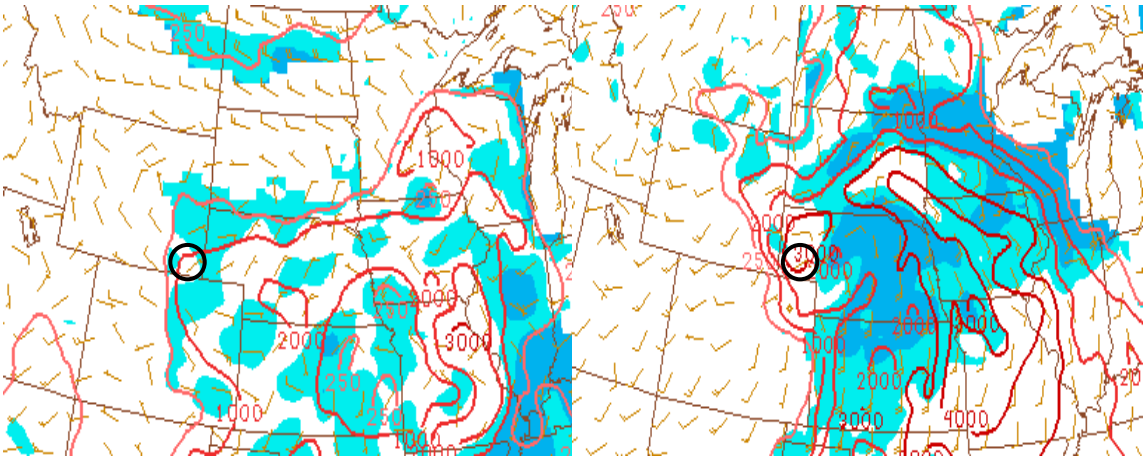

a) **b)**

Figure 6.5: MLCAPE for- a) 15 June and b) 21 June. The oval indicates the approximate location storms developed on each day.

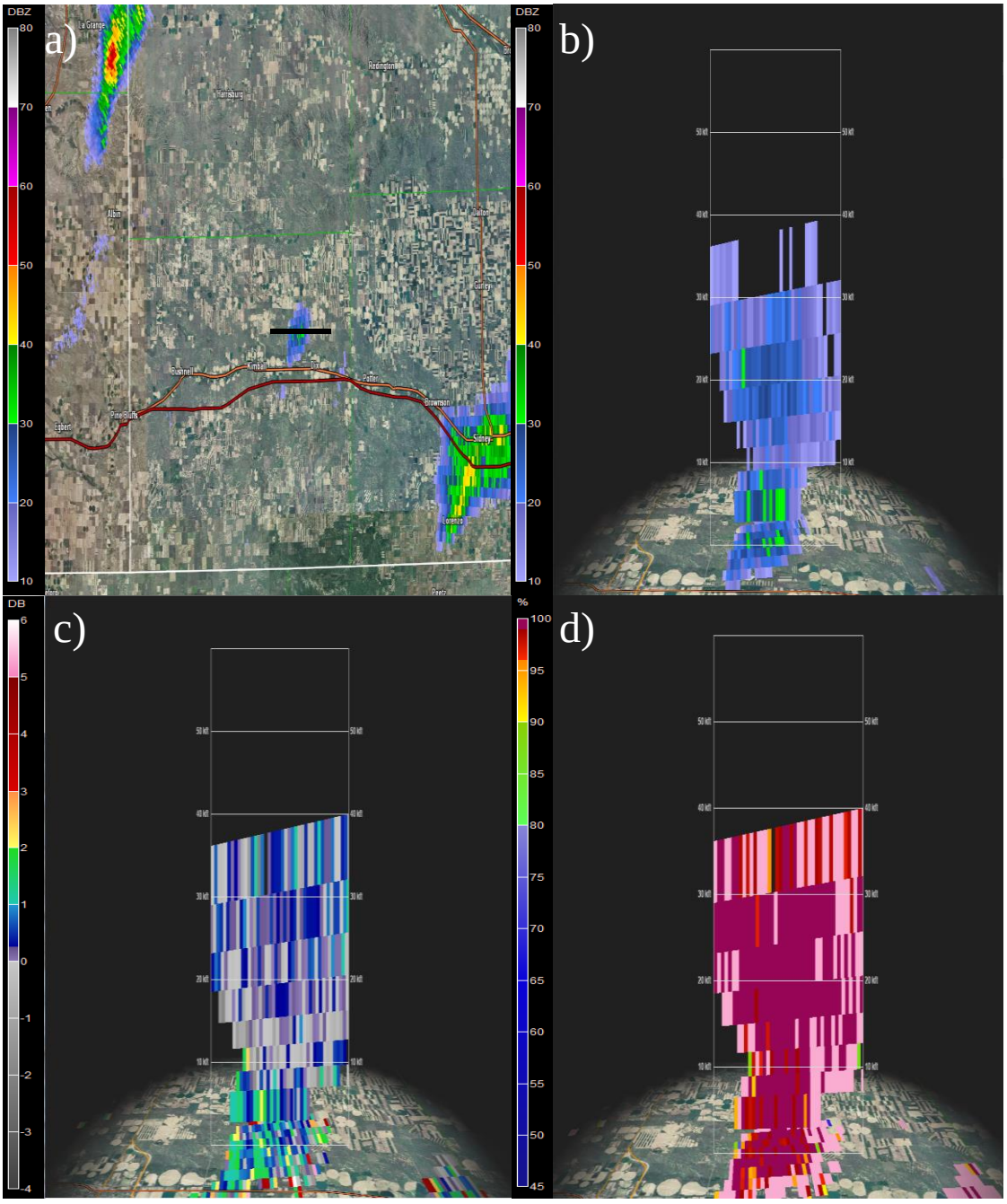

Figure 6.6: a) Reflectivity image at 2001 UTC on 21 June 2013 with the solid line denoting the cross-section location; b) vertical cross-section of reflectivity; c) vertical cross-section of differential reflectivity; and d) vertical cross-section of correlation coefficient. The horizontal lines in the cross-section represent height intervals of every 10,000ft.

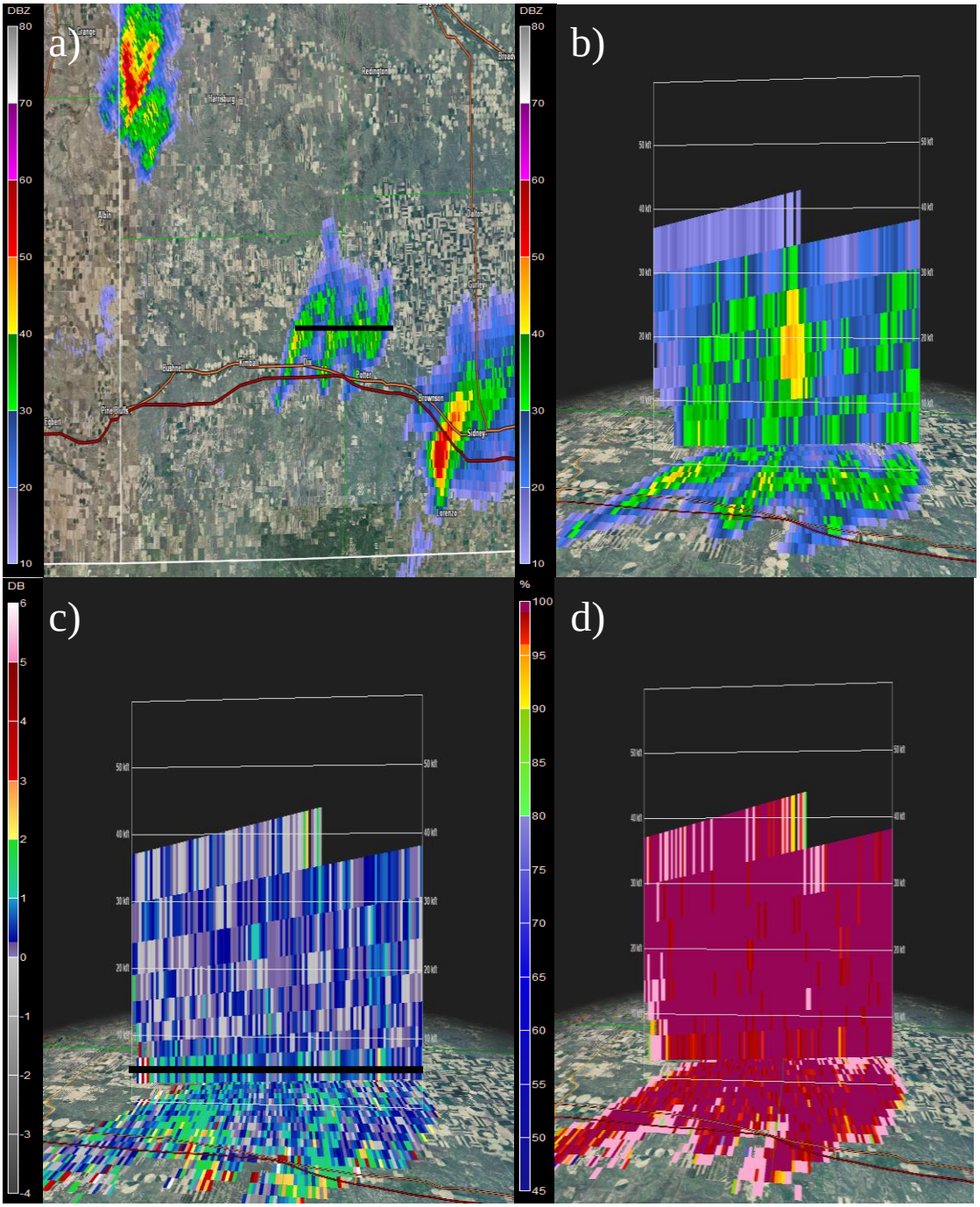

Figure 6.7: Same as in figure 6.6 but at 2020 UTC on 21 June 2013. The solid line panel c denotes the approximate location of the 1500 m height level.

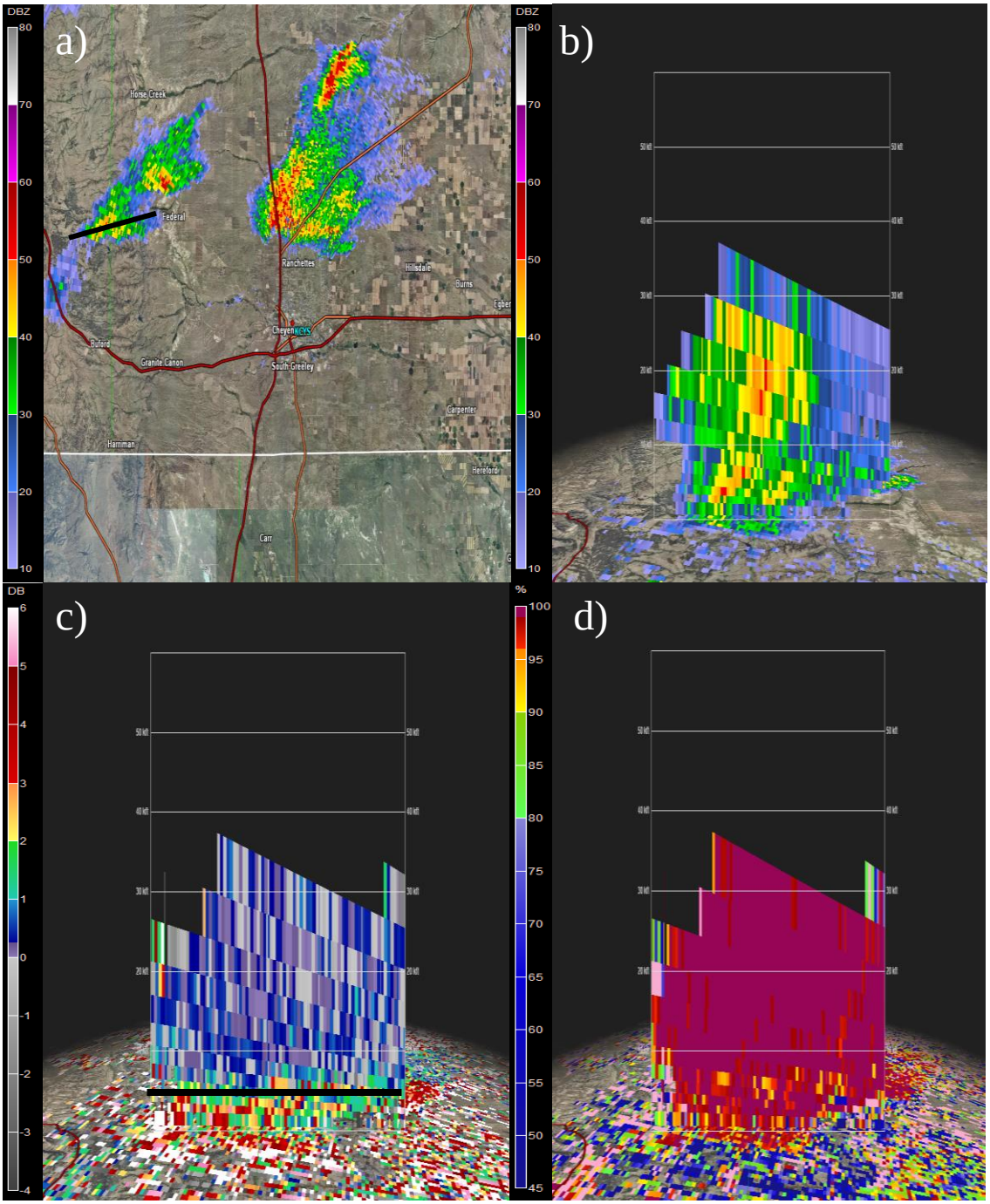

Figure 6.8: a) Reflectivity image at 2150 UTC on 15 June 2013 with the solid line denoting the cross-section location; b) vertical cross-section of reflectivity; c) vertical cross-section of differential reflectivity; and d) vertical cross-section of correlation coefficient. The horizontal lines in the cross-section represent height intervals of every 3000 m. The solid line in panel c denotes the approximate location of the 1500 m height level.

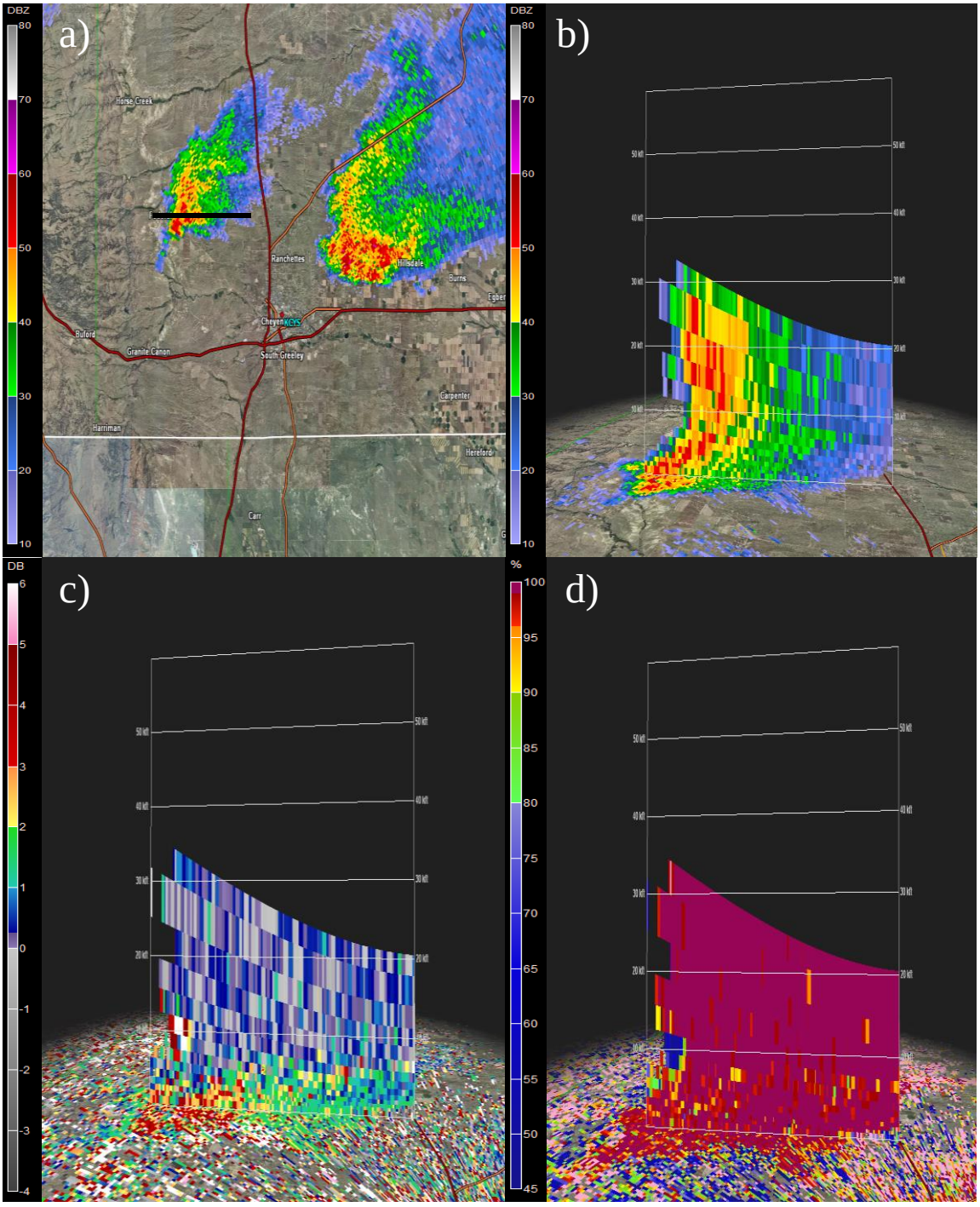

Figure 6.9: Same as figure 6.8 but at 2220 UTC on 15 June 2013.

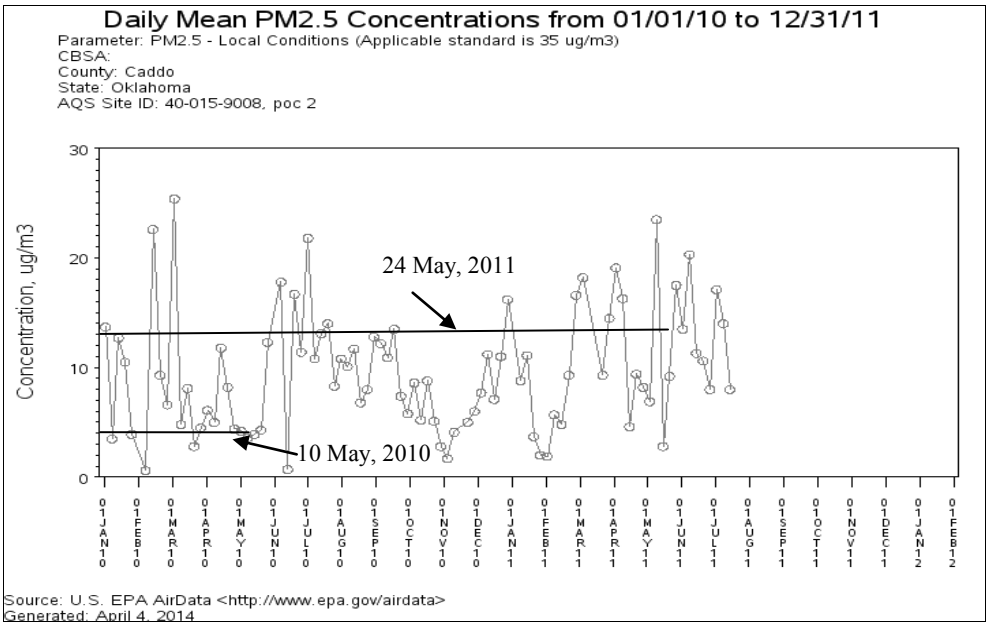

a)

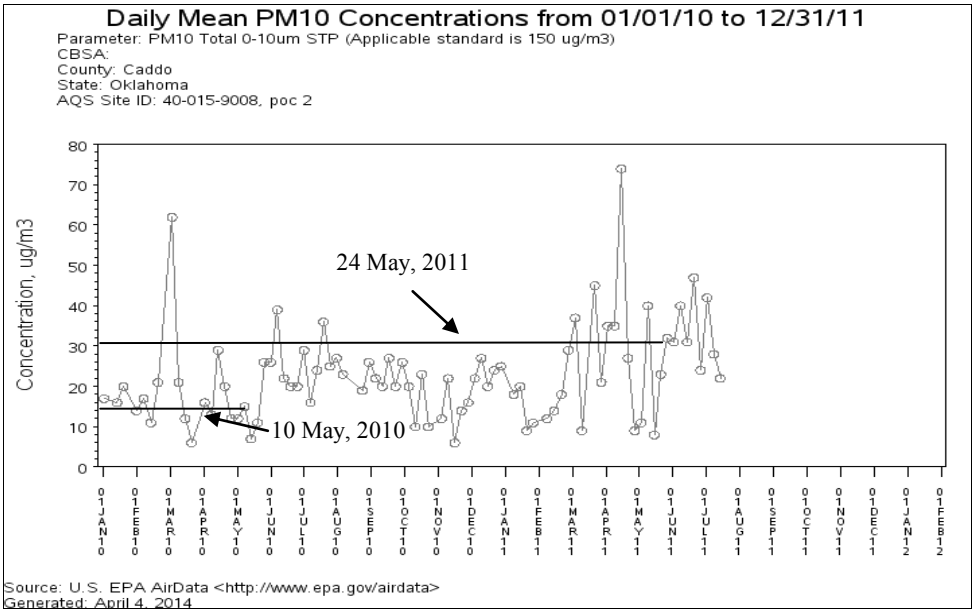

b)

Figure 6.10: a) PM2.5 concentration for Caddo County, OK for 10 May 2010 and 24 May 2011; and b) PM10 concentration for Caddo County, OK for 10 May 2010 and 24 May 2011

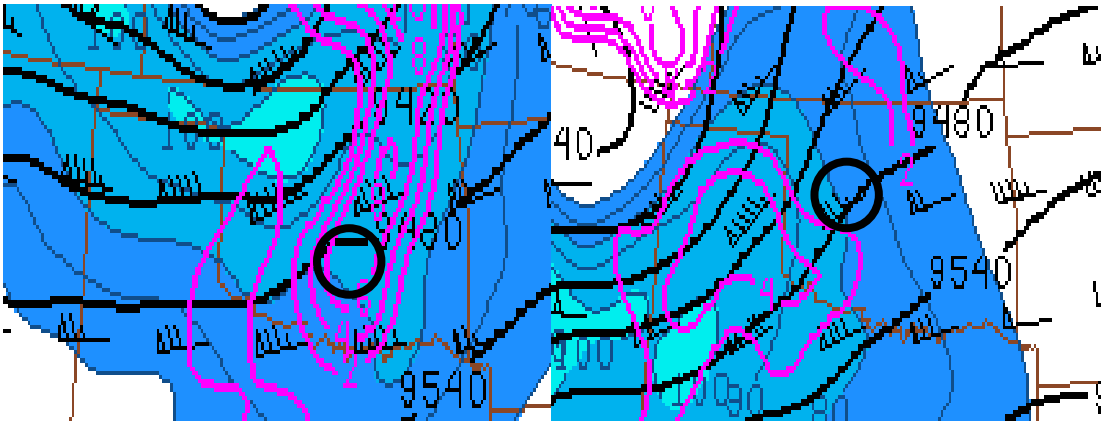

a) **b)**

Figure 6.11: 300 mb flow for- a) 10 May 2010 and b) 24 May 2011. The oval indicates the approximate location storms developed on each day.

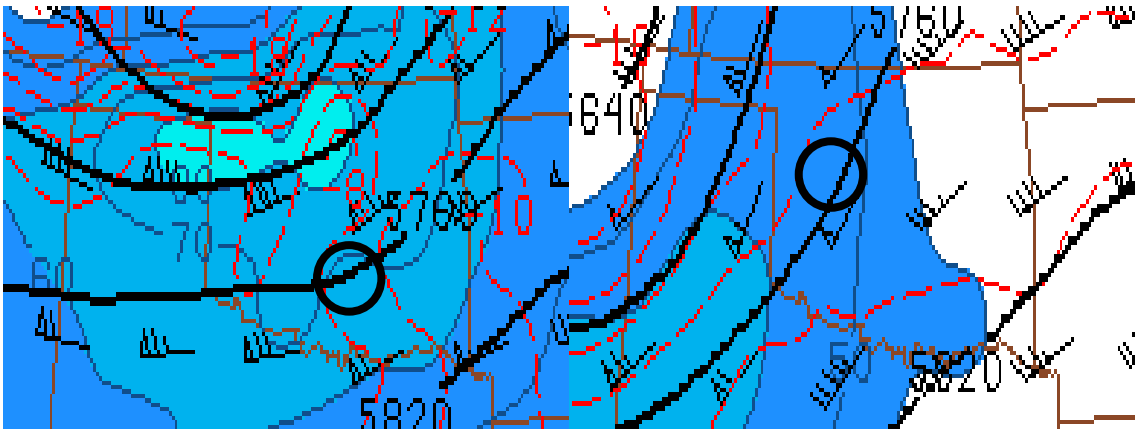

a) **b)**

Figure 6.12: As in figure 6.14, except for the 500 mb flow.

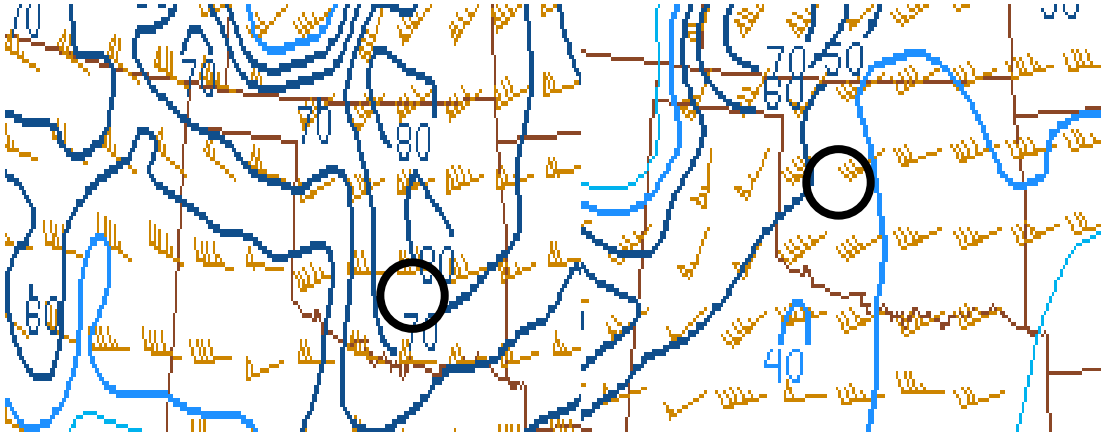

a) **b)**

Figure 6.13: 0-6 km bulk shear for- a) 10 May 2010 and b) 24 May 2011. The oval indicates the approximate location storms developed on each day.

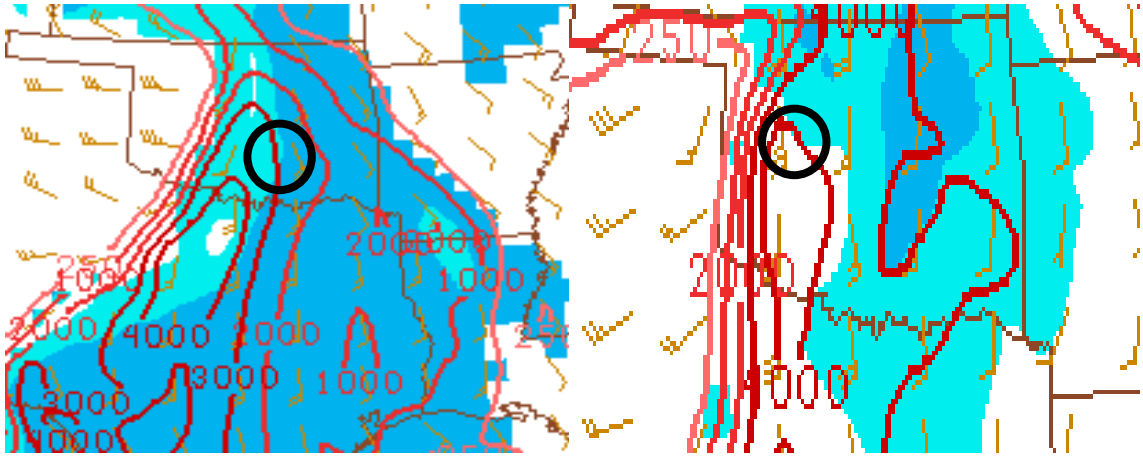

a) **b)**

Figure 6.14: MLCAPE for- a) 10 May 2010 and b) 24 May 2011. The oval indicates the approximate location storms developed on each day.

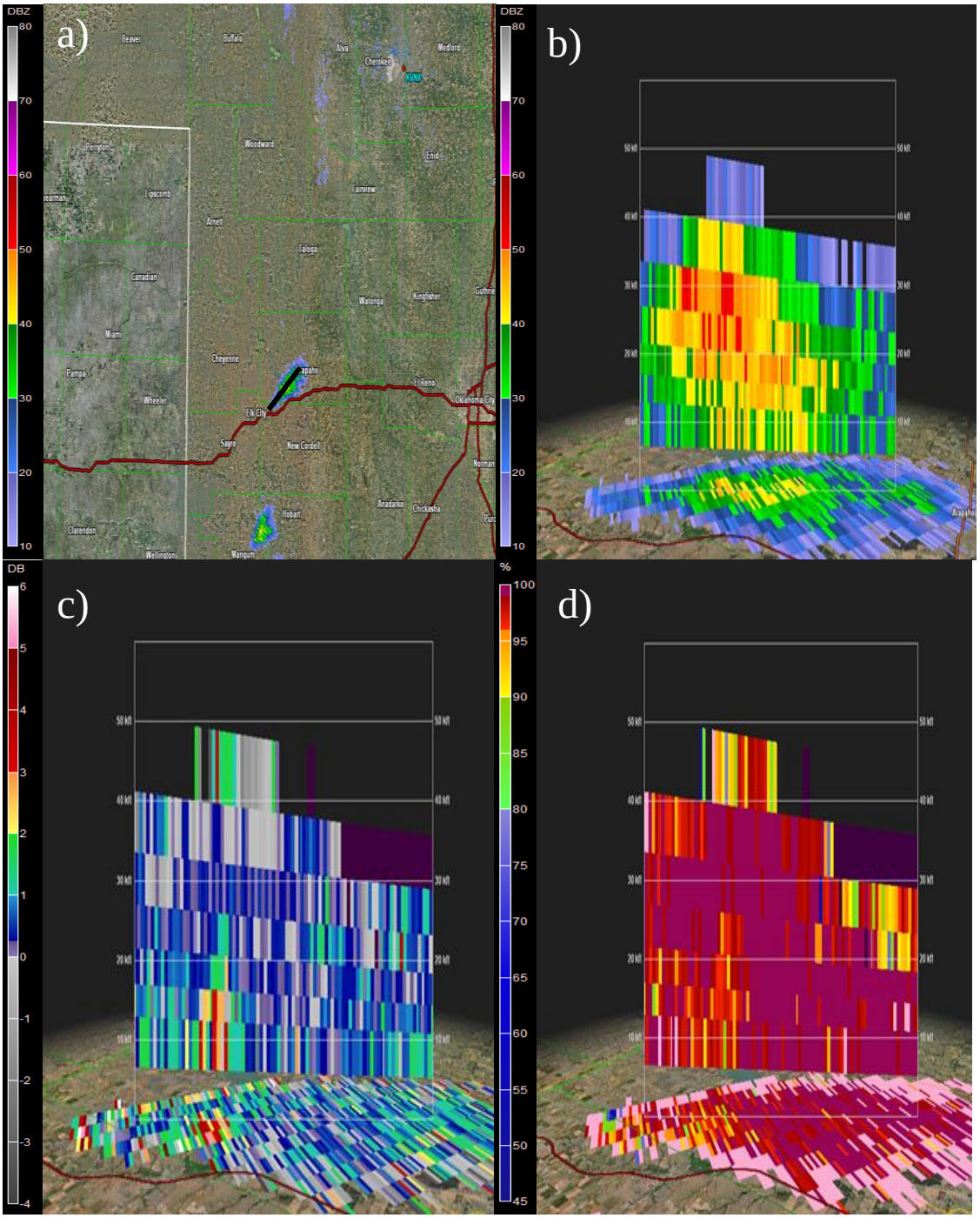

Figure 6.15: a) Reflectivity image at 1852 UTC on 24 May 2011 with the solid line denoting the cross-section location; b) vertical cross-section of reflectivity; c) vertical cross-section of differential reflectivity; and d) vertical cross-section of correlation coefficient. The horizontal lines in the cross-section represent height intervals of every 3000 m.

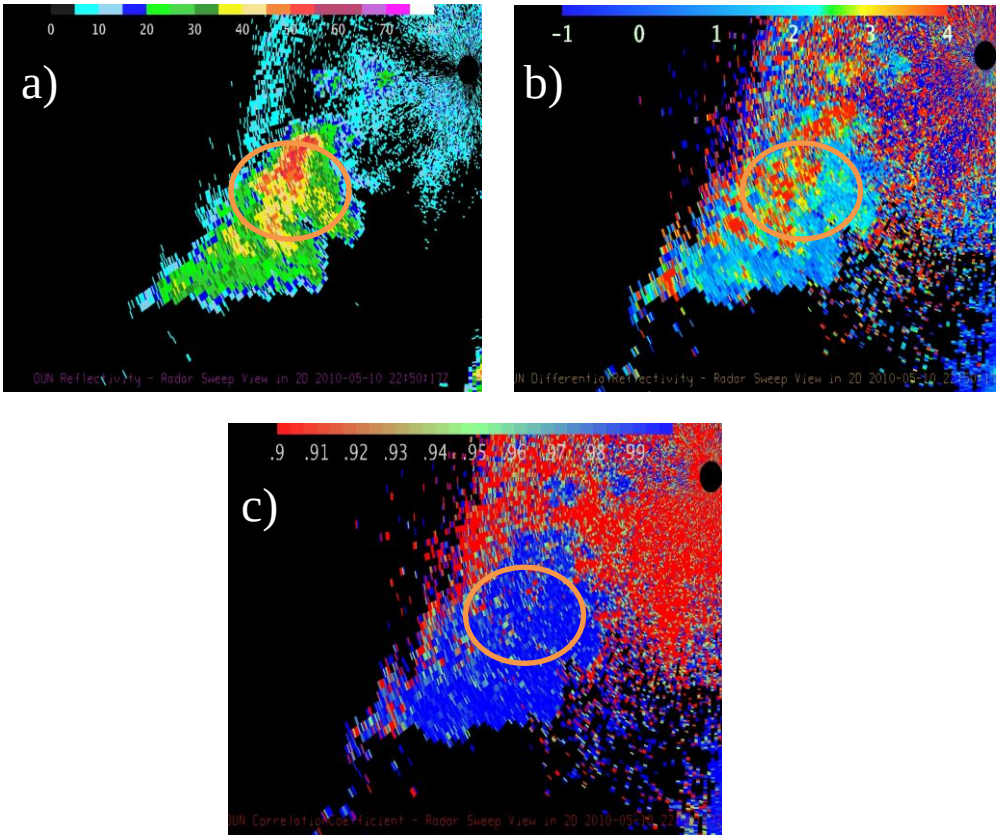

Figure 6.16: a) Reflectivity image at 2250 UTC on 10 May 2010 at approximately 1.5 km above b) differential reflectivity at approximately 1.5 km above surface and c) correlation coefficient at approximately 1.5 km above surface. The 1.5 km elevation applies to the encircled area.

7. Conclusions

In this study, we have presented a preliminary observational study of the effects of aerosols on convection over the Great Plains of the United States as we seek to provide evidence for or against an aerosol impact on convection. This was accomplished using storm reports and polarimetric radar data. Some of the primary conclusions reached are:

A. A new method was developed to identify the relative concentration of biomass burning particles. Using the bootstrapping technique to reduce the effects of a limited storm reports sample size, statistically significant larger hail size and stronger surface wind speeds were found with higher aerosol concentration ($p<0.001$). The results suggest that aerosols may have an impact on convective intensity. The first limitation is only having eleven years of aerosol data, with aerosol measurements 3 days apart. This limited data produced a small sample size of storm reports within each aerosol concentration category, as the number of days in each aerosol concentration category was substantially reduced. Another limitation is that despite considering only the days with similar thermodynamic and kinematic environments, storm type (e.g., supercell, multicell, squall line) was not taken into account when constructing the distribution of hail size and wind speed as a function of aerosol concentration. Storm mode could have a significant impact on the behavior of hail size and wind speed as a function of aerosol concentration. Future work should examine how updraft and downdraft

strength change in similar storm types between days of different aerosol concentration. This would provide further insight into how the strength of different storm hazards (e.g., hail size, damaging winds, and tornado winds) would change.

B. A composite synoptic regime was obtained for each aerosol concentration category at the surface and 500 hPa. At the surface, northerly winds were common during low aerosol days along the Central Plains as the composite low pressure center was located farther east, into Illinois. Southerly winds originating from the Yucatan Peninsula and western Gulf of Mexico were more common during medium and high aerosol days across the Central Plains as the composite low pressure center was located farther west, into the central and southern High Plains. Even though the magnitude and direction of the composite surface flow was similar between medium and high aerosol days, the maximum in the composite surface flow extended further north during high aerosol days. This was most likely as a result of a stronger surface low observed on high aerosol days. The stronger surface low observed on high aerosol days may have been as a result of a greater amplification of the 500 hPa trough.

C. 4-day backward parcel path trajectories were obtained for all days for each aerosol concentration category. Parcels were analyzed at 100 m and 300 m, corresponding to the flow near the surface. The path location was examined 2 and

4 days prior to the aerosol observation day. It was found that during low aerosol days, parcels originated from the north region. On medium and high aerosol days, parcels more often originated from the western Gulf of Mexico. Even though there were more cases in which parcels originate from the Yucatan Peninsula/western Caribbean region during high aerosol days, this does not represent a high percentage of days in this category. The limitation illustrated by this observation that all the biomass burning characteristics were identified for the savanna landscape that composes most of southern Mexico and the Yucatan Peninsula. Smoke from wildfires, however, can be advected from other regions such as northwestern Mexico or the Desert Southwest. The smoke characteristics from these other regions may be slightly different due to a different vegetation community producing the smoke. A complicating factor was that parcels during the days prior to the aerosol observation day examined were ascending and descending to different vertical levels. The wind direction could vary at these different height levels, significantly influencing parcel trajectory. Another complicating factor is that even though the 100 m and 300 m level are close to each other, parcels at each of these levels were more widely separated from each other at 4 days prior to the aerosol observation day. This raises uncertainty in the parcel trajectory the further back in time the backward trajectories are performed.

D. Polarimetric radar data was used to examine differences in inferred thunderstorm microphysics between days of different aerosol concentrations for

High Plains and Oklahoma storms. It was found that during the higher aerosol days for both regions, differential reflectivity was lower and correlation coefficient was higher, suggesting the presence of a larger concentration of smaller droplets. It was also found, however, that there may have been more of an aerosol effect on the High Plains cases than in the Oklahoma cases due to different environmental conditions. Future work should compare additional polarimetric radar data between days of different aerosol concentration with similar environmental parameters to make this part of the study more robust, since it was limited by the small number of available cases due to the recent polarimetric upgrade on all WSR-88D radars.

References

Albrecht, B.A., 1989: Aerosols, cloud microphysics, and fractional cloudiness. *Science,* **245**, 1227-1230.

Andreae, M.O., D. Rosenfeld, P. Artaxo, A.A. Costa, G.P. Frank, K.M. Longo, and M.A.F. Silva- Dia, 2004: Smoking rain clouds over the Amazon. *Science*, **303**, 1337-1342.

Battan, L. J., and R. R. Braham, 1956: A study of convective precipitation based on cloud and radar observations. *J. Meteor.*, **13**, 587–591.

Beard, K. V., J. Q. Feng, and C. Chuang (1989a), A simple perturbation model for the electrostatic shape of falling drops, J. Atmos. Sci., 46, 2404–2418.

Bell, T. L., D. Rosenfeld, K.M. Kim, J.M. Yoo, M.I. Lee, and M. Hahnenberger, 2008: Midweek increase in U.S. summer rain and storm heights suggests air pollution invigorates rainstorms. *J. Geophys. Res.*, **113**, D02209.

Bell, T.L., D. Rosenfeld, and K.M. Kim, 2009: Weekly cycle of lightning: Evidence of storm invigoration by pollution. *Geophys. Res. Lett.*, **36**, L23805.

Cober, S. G., and R. List 1993, Measurements of the heat and mass transfer parameters characterizing conical graupel growth. *J. Atmos. Sci.,* **50**, 1591–1609.

Echalar, F., A. Gaudichet, H. Cachier, and P. Artaxo, 1995: Aerosol emissions by tropical forest and savanna biomass burning: characteristic trace elements and fluxes. *Geophys. Res. Lett.,* **22(22)**, 3039-3042.

Efron, B., 1979: Bootstrap methods: Another look at the jackknife. *'Ann. Statist.' 7*, 1-26, doi:10.1214/aos/1176344552http://projecteuclid.org/euclid.aos/1176344552.

Givati, A., and D. Rosenfeld, 2004: Quantifying precipitation suppression due to air pollution. *J. Appl. Meteor.,* **43,** 1038–1056.

IMPROVE, 1995: IMPROVE Data Guide. [Available online at http://vista.cira.colostate.edu/improve/publications/OtherDocs/IMPROVEDataGuide/IMPROVEdataguide.htm]

IMPROVE, 2006: Chapter 1: Improve Network- Purpose, Design, and History. [Available online at http://vista.cira.colostate.edu/improve/publications/reports/2006/PDF/Chapter1.NetworkOverview.pdf]

Jirak, I. L., and W. R. Cotton, 2006: Effect of air pollution on precipitation along the Front Range of the Rocky Mountains. *J. Appl. Meteor. Climatol.,* **45,** 236–245.

Kauffman, Y. J., I. Koren, L.A. Remer, D. Rosenfeld, and Y. Rudich, 2005: The effect of smoke, dust, and pollution aerosol on shallow cloud development over the Atlantic Ocean. *Proc. Natl. Acad. Sci. USA*, **102(32)**, 11207-11212.

Khain, A., D. Rosenfeld, A. Pokrovsky, 2005: Aerosol impact on the dynamics and microphysics of deep convective clouds, *Q.J.Roy. Meteor. Soc.,* **131**, 2639-2663, doi:10.1256/qj.04.62.

Khain, A., N. BenMoshe, and A. Pokrovsky, 2008: Factors determining the impact of aerosols on surface precipitation from clouds: An attempt at classification. *J. Atmos. Sci.,* **65**, 1721–1748.

Khain, A., D. Rosenfeld, A. Pokrovsky, U. Blahak, and A. Ryzhkov, 2010: The role of CCN in precipitation and hail in a mid- latitude storm as seen in simulations using a spectral (bin) microphysics model in a 2D dynamic frame. *Atmos. Res.*, **99**, 129–146, doi:10.1016/j.atmosres.2010.09.015.

Lerach, D.G., B.J. Gaudet, and W.R. Cotton, 2008: Idealized simulations of aerosol influences on tornadogenesis. *Geophys. Res. Lett.*, **35**, L23806, doi:10.1029/2008GL035617.

Lerach, David G., William R. Cotton, 2012: Comparing aerosol and low-level moisture influences on supercell tornadogenesis: Three-dimensional idealized simulations. *J. Atmos. Sci.,* **69**, 969–987.

Li, Z., N. Feng, J. Fan, Y. Liu, D. Rosenfeld, and Y. Ding, 2011: Long-term impacts of aerosols on the vertical development of clouds and precipitation. *Nature Geoscience,* **4**, 888-894.

Lin, J.C., T. Matsui, R.A. Pielke, and C. Kummerow, 2006: Effects of biomass-burning-derived aerosols on precipitation and clouds in the Amazon Basin: A satellite-based empirical study. *J. Geophys. Res.,* **111**, D19204, doi:19210.11029/12005JD006884.

Lynn, B. H., A. Khain, J. Dudhia, D. Rosenfeld, A. Pokrovsky, and A. Seifert, 2005a: Spectral (bin) microphysics coupled with a mesoscale model (MM5). Part I: Model description and first results. *Mon. Wea. Rev.,* **133,** 44–58.

Lynn, B. H., A. Khain, J. Dudhia, D. Rosenfeld, A. Pokrovsky, and A. Seifert, 2005b: Spectral (bin) microphysics coupled with a mesoscale model (MM5). Part II: Simulation of a CaPE rain event with squall line. *Mon. Wea. Rev.,* **133,** 59–71.

Lynn, B. H., A. Khain, D. Rosenfeld, and W. Woodley, 2007: Effects of aerosols on precipitation from orographic clouds. *J. Geophys. Res.,* **112,** D10225, doi:10.1029/2006JD007537.

Lyons, W.A., T.E. Nelson, E.R. Williams, J.A. Cramer, and T.R. Turner, 1998: Enhanced positive cloud-to-ground lightning in thunderstorms ingesting smoke from fires. *Science,* **282**, 77-80.

Mansell, E.R., C.L. Ziegler, 2013: Aerosol effects on simulated storm electrification and precipitation in a two-moment bulk microphysics model. *J. Atmos. Sci.*, **70**, 2032–2050. doi: http://dx.doi.org/10.1175/JAS-D-12-0264.1.

May, P. T., V. N. Bringi, M. Thurai, 2011: Do we observe aerosol impacts on DSDs in strongly forced tropical thunderstorms? *J. Atmos. Sci.*,**68**, 1902–1910. doi: http://dx.doi.org/10.1175/2011JAS3617.1.

Reid, J.S., E.M. Prins, D. L. Westphal, C. C. Schmidt, K. A. Richardson, S. A. Christopher, T. F. Eck, E. A. Reid, C. A. Curtis, and J. P. Hoffmann, 2004: Real-time monitoring of South American smoke particles emissions and transport using a coupled remote sensing/box-model approach. *Geophys. Res. Lett.*, **31**, L06107, doi:06110.01029/02003GL018845.

Rose, D., A. Nowak, P. Achtert, A. Wiedensohler, M. Hu, M. Shao, Y. Zhang, M. O. Andreae, and U. Pöschl, 2010: Cloud condensation nuclei in polluted air and biomass burning smoke near the mega-city Guangzhou, China – Part 1: Size-resolved measurements and implications for the modeling of aerosol particle hygroscopicity and CCN activity. *Atmos. Chem. Phys.*, **10**, 3365-3383, doi:10.5194/acp-10-3365-2010, 2010.

Rosenfeld, D., 1999: TRMM observed first direct evidence of smoke from forest fires inhibiting rainfall. *Geophys. Res. Lett.,* **26(20)**, 3105-3108.

Rosenfeld, D., and T.L Bell, 2011: Why do tornadoes and hailstorms rest on weekends? *J. Geophys. Res. Lett.*, **116**, D20211.

Rosenfeld, D., and T.L Bell, 2013: Reply to comment by S.E. Yuter et al. on "Why do tornadoes and hailstorms rest on weekends?" *J. Geophys. Res Atmos.*, **118(13)**, doi: 10.1002/jgrd.50539.

Storer, R.L., S. C. van den Heever, 2013: Microphysical processes evident in aerosol forcing of tropical deep convective clouds. *J. Atmos. Sci.*, **70**, 430–446. doi: http://dx.doi.org/10.1175/JAS-D-12-076.1.

Straka, J. M., D. S. Zrnic, and A. V. Ryzhkov, 2000: Bulk hydrometeor classification and quantification using multiparameter radar data: Synthesis of relations. *J. Appl. Meteor.*, **39**, 1341–1372.

Tao, W.-K., X. Li, A. Khain, T. Matsui, S. Lang, and J. Simpson, 2007: Role of atmospheric aerosol concentration on deep convective precipitation: Cloud-resolving model simulations. *J. Geophys. Res.*, **112**, D24S18, doi:10.1029/2007JD008728.

Twomey, S., 1974: Pollution and the planetary albedo. *Atmos. Environ.*, **8**, 1251-1256.

Yuan, T., L. Remer, K.E. Pickering, and H. Yu, 2011: Observational evidence of aerosol enhancement of lightning activity and convective invigoration. *Geophys. Res. Lett.*, **38**, L04701, doi:10.1029/2010GL046052.

Yuter, S. E., M. A. Miller, M. D. Parker, P. M. Markowski, Y. Richardson, H. Brooks, and J. M. Straka, 2013: Comment on “Why do tornados and hailstorms rest on weekends?” by D. Rosenfeld and T. Bell. *J. Geophys. Res. Atmos.,* **118**, doi:10.1002/jgrd.50526.

Wang J., S.C. van den Heever, and J.S. Reid, 2009: A conceptual model for the link between Central American biomass burning aerosols and severe weather over the south central United States. *Environ. Res. Lett.*, **4**, 015003, doi:10.1088/1748-9326/4/1/015003.

Wang, J., S. A. Christopher, U. S. Nair, J. S. Reid, E. M. Prins, J. Szykman, and J. L. Hand, 2006: Mesoscale modeling of Central American smoke transport to the United States, Part I: "Top-down" assessment of emission strength and diurnal variation impact. *J. Geophys. Res.*, **111**, D05S17, doi:10.1029/2005jd006720.